

# The mass range for hot subdwarf B stars from MESA simulations: dependence on metallicity and overshooting

---

EDUARDO ARANCIBIA ROJAS

Supervisor: Dr. Mónica Zorotovic (Universidad de Valparaíso - Chile)

Co-supervisor: Dr. Maja Vučković (Universidad de Valparaíso - Chile)

External reviewer: Alexey Bobrick (Technion – Israel Institute of Technology)



Tesis para optar al grado de Magíster en Astrofísica  
Instituto de Física y Astronomía  
Facultad de Ciencias  
Universidad de Valparaíso

---

Abril 2023  
Valparaíso, Chile.



---

This thesis is solely my own composition,  
except where specifically indicated in the text.

Total or partial reproduction, for scientific or academic purposes,  
is authorised including a bibliographic reference to this document.

Eduardo Arancibia Rojas

Abril 2023

Valparaíso, Chile.



# Agradecimientos

En primer lugar deseo expresar mi agradecimiento a la Dra. Mónica Zorotovic por el apoyo, orientación y compromiso durante todo el proceso de investigación y redacción de mi tesis. Su paciencia, experiencia y conocimientos han sido invaluable para el éxito de mi trabajo. Quiero agradecerle por haberme brindado la oportunidad de realizar esta tesis y por haberme confiado la responsabilidad de llevar a cabo una investigación en un tema que es de gran importancia para mí. Además, sus sugerencias y comentarios constructivos me han ayudado a mejorar mi enfoque y a obtener mejores resultados. Me siento muy afortunado de haber tenido a una asesora tan dedicada, que siempre estuvo dispuesta a responder mis preguntas, aclarar mis dudas y proporcionarme los recursos necesarios para avanzar en mi investigación. Sin su guía y apoyo, este proyecto habría sido mucho más difícil de llevar a cabo.

También quiero agradecer a la Dra. Maja Vuckovic y Dr. Alexey Bobric, por su colaboración y contribución a mi investigación. Sus comentarios y sugerencias fueron fundamentales para perfeccionar el resultado final de esta investigación.

Agradecer por el financiamiento del proyecto FONDECYT regular 1211941, proporcionado por la Dra. Maja Vuckovic, y al programa de Postgrado en Astrofísica del Instituto de Física y Astronomía de la Universidad de Valparaíso por la beca de manutención recibida durante mi programa de magíster.

Por último, me gustaría agradecer a mi familia y amigos, en especial a mi madre Mireya Damaris Rojas Tapia por su constante apoyo emocional durante este proceso. Su amor y aliento me han mantenido motivado y enfocado en mi objetivo. Le agradezco de todo corazón por su tiempo, dedicación y sabiduría. Este logro no habría sido posible sin su ayuda y orientación.



# Abstract

Hot subdwarf B (sdB) stars are helium core burning stars that have lost almost their entire hydrogen envelope due to binary interaction. Their assumed canonical mass of  $M_{\text{sdB}} \sim 0.47 M_{\odot}$  has recently been debated given a broad range found both from observations as well as from the simulations.

The mass range for sdBs as a function of initial mass was derived two decades ago by Han et al. (2002), using the Eggleton code, for two different metallicities ( $Z = 0.02$  and  $Z = 0.004$ ). Here, I revised and refined these calculations, using the stellar evolution code MESA. An excellent agreement was obtained for low-mass progenitors, up to  $\sim 2.0 M_{\odot}$ . For more massive progenitors, a direct comparison was not possible due to the different prescription for overshooting these authors used, which is not available in MESA. However, I found that in general the MESA models result in a wider mass range compared to the simulations performed by Han et al. (2002) with the Eggleton code, for more massive stars.

The effects of metallicity and the inclusion of core overshooting during the main sequence were also analysed. I found that the lower metallicity models predict, on average, slightly more massive sdBs ( $0.01 - 0.02 M_{\odot}$  larger). The inclusion of core overshooting during the main sequence mostly affected progenitors more massive than  $\sim 1.5 M_{\odot}$ , as expected, decreasing the maximum initial mass for which the core becomes degenerate during the red giant branch phase, and increasing the sdB mass for progenitors that ignite helium under non-degenerate conditions.

The duration of the sdB phase was also calculated, finding a strong anti-correlation with the sdB mass.

Finally, I discussed several factors that might affect the sdB mass distribution and should be considered in binary population synthesis models that aim to compare with observational samples.



# Contents

<b>1</b>	<b>Introduction</b>	<b>1</b>
<b>2</b>	<b>Reviewing the work from Han et al. (2002)</b>	<b>7</b>
2.1	Comparison with SSE . . . . .	10
<b>3</b>	<b>Models with MESA</b>	<b>15</b>
3.1	From pre-MS to TAMS . . . . .	16
3.2	From TAMS to the tip of the RGB . . . . .	18
3.3	Removing the envelope during the RGB phase and evolving until the white dwarf cooling track . . . . .	18
3.4	Finding the minimum sdB masses . . . . .	19
3.5	Results . . . . .	20
3.5.1	SdB masses for solar metallicity ( $Z = 0.02$ ) . . . . .	27
3.5.2	SdB masses for lower metallicity ( $Z = 0.004$ ) . . . . .	31
<b>4</b>	<b>Discussion</b>	<b>35</b>
4.1	Comparison with the results from Han et al. (2002) . . . . .	35
4.2	Lifetimes of the sdBs . . . . .	39
4.3	Implications for binary modelling . . . . .	41
<b>5</b>	<b>Summary and Future Work</b>	<b>45</b>
<b>A</b>	<b>MESA inlists</b>	<b>49</b>
A.1	Pre-MS to TAMS . . . . .	49
A.2	TAMS to the tip of the RGB . . . . .	51
A.3	Removing the envelope and evolving until the white dwarf cooling track	53
<b>B</b>	<b>Tables</b>	<b>57</b>
B.1	SdB properties for solar metallicity without overshooting . . . . .	58

## CONTENTS

---

B.2	SdB properties for solar metallicity with overshooting . . . . .	59
B.3	sdB properties for $Z = 0.004$ metallicity with overshooting . . . . .	60

# CHAPTER 1

## Introduction

Hot subluminous blue stars were discovered in the middle of the XX century (e.g., Luyten, 1953; Greenstein, 1956; Münch, 1958) based on the Humason & Zwicky (1947) photometric survey of the North Galactic Pole and Hyades regions. Nowadays, we know that these stars, called *hot subdwarf B* (sdB) stars, have lost virtually all of their hydrogen envelopes, being composed of a helium-burning core and a very thin layer of hydrogen. The envelope must have been lost close to the tip of the Red giant branch (RGB) phase, in order to allow the core to grow massive enough to ignite helium. They are called subdwarfs due to their location on the Hertzsprung Russell (HR) diagram, below the main sequence (MS) where stars spend most of their lives. Stars with masses  $\leq 10 M_{\odot}$  on the MS are often called dwarf stars, hence the term subdwarfs. This term was coined by Gerard Peter Kuiper (Kuiper, 1939). Their luminosity class is VI in the Morgan-Keenan classification (Morgan et al., 1943). Figure 1.1 shows the location of subdwarf stars on the HR diagram. There are cool subdwarfs with spectral types G to M, while hot subdwarfs are much hotter with spectral types B (if the effective temperature is between  $\sim 20\,000$  K and  $\sim 40\,000$  K) and O (with  $\sim 40\,000$  to  $\sim 100\,000$  K). The sdB stars lie in the region also called ‘Extreme horizontal branch’ (EHB), which is an extension of the region occupied by evolved core-helium-burning stars. They have a radius between  $0.15$  and  $0.25 R_{\odot}$  and a typical mass of about half a solar mass. However, given their larger effective temperatures, they are 10 – 100 times brighter than the Sun.

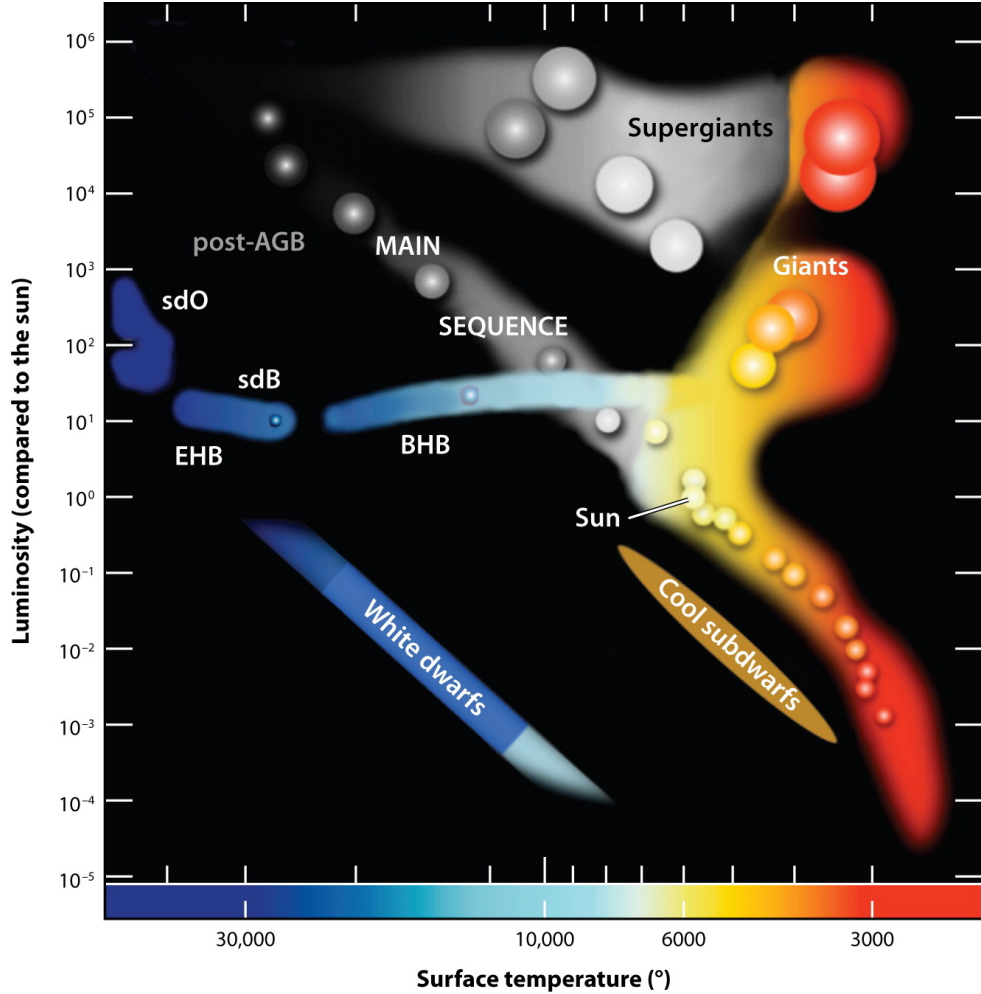


**Figure 1.1:** The Hertzsprung Russell diagram, reproduced from Heber (2009), shows the different evolutionary phases of stars and indicates the regions where we can find the cool subdwarf stars as well as the hot subdwarfs type B and O.

The duration of the sdB phase is of the order of a hundred Myr and depends mostly on the mass of the sdB (e.g., Iben & Tutukov, 1985; Yungelson, 2008). When an sdB star stops burning helium in the core, it will establish helium burning in a shell. This causes an increase in the effective temperature ( $T_{\text{eff}} > 35\,000\text{ K}$ ) and luminosity, moving the star in the HR diagram to the location where subdwarf O (sdO) stars reside. However, since there is not enough hydrogen in the envelope, the star will not reach the asymptotic giant branch (AGB), which is why these stars are also known as ‘failed AGB stars’ and later on will follow the cooling track of carbon/oxygen or hybrid helium/carbon/oxygen white dwarfs (e.g., Zenati et al., 2019). The duration of the sdO

---

phase for post-sdB stars is typically an order of magnitude shorter than the sdB phase (about 10 Myr; Justham et al., 2010).

SdB stars are produced through binary stellar interactions, which is necessary for the progenitor star to lose its hydrogen envelope (Pelisoli et al., 2020). There are three main binary evolutionary channels that allow us to explain this process: i) stable Roche Lobe Overflow (RLOF); ii) common envelope channel (often denoted as ‘CE’); and iii) merger of two helium white dwarfs.

i) **The stable Roche Lobe Overflow:** This channel, shown in the middle panel in Figure 1.2, requires an initially relatively close binary system (initial orbital periods  $\sim 100 - 800$  d) composed of two stars with a mass ratio smaller than  $M_{\text{donor}}/M_{\text{accretor}} \sim 2.0$  (Vos et al., 2020). The more massive star evolves to the giant phase and fills its Roche lobe due to the expansion of its envelope close to the tip of the RGB. Given the small mass ratio, mass transfer to the companion remains stable. When the mass of the hydrogen envelope has decreased sufficiently, helium is ignited in the core and the radius of the giant star begins to contract causing mass transfer to stop. This forms an sdB star in a wide binary system with a MS or subgiant (SG) star companion.

ii) **The Common Envelope:** In this scenario (left panel in Figure 1.2) the initial binary has a larger mass ratio. The more massive star evolves to the RGB phase and fills its Roche lobe. Due to the deep convective envelope of the RGB star and the large mass ratio, mass transfer can accelerate and quickly becomes dynamically unstable, causing a common envelope phase (Paczynski, 1976). In this very short phase, the envelope of the donor encompasses both the degenerate core of the RGB star and its companion. Drag forces reduce the distance between the two stars in a spiral-in process. If the system survives the common envelope phase without merging, it will result in a close binary, composed of the degenerate core of the star that ejected the envelope and its still main-sequence companion. It is this core that can form an sdB star if it is massive enough to ignite helium after the envelope ejection.

SdBs can also result from a combination of the stable and unstable Roche Lobe overflow processes just described, which might result in short-period binaries with white dwarf companions (right panel in Figure 1.2). In this case, the white dwarf should have formed first, probably due to stable Roche lobe overflow during the RGB phase leading to a low-mass helium-core white dwarf. The sdB progenitor evolves later and fills the Roche lobe during the RGB phase. As the companion has already lost all its envelope, the donor to accretor mass ratio is high enough to ensure unstable mass transfer and the development of a common envelope phase, which dramatically

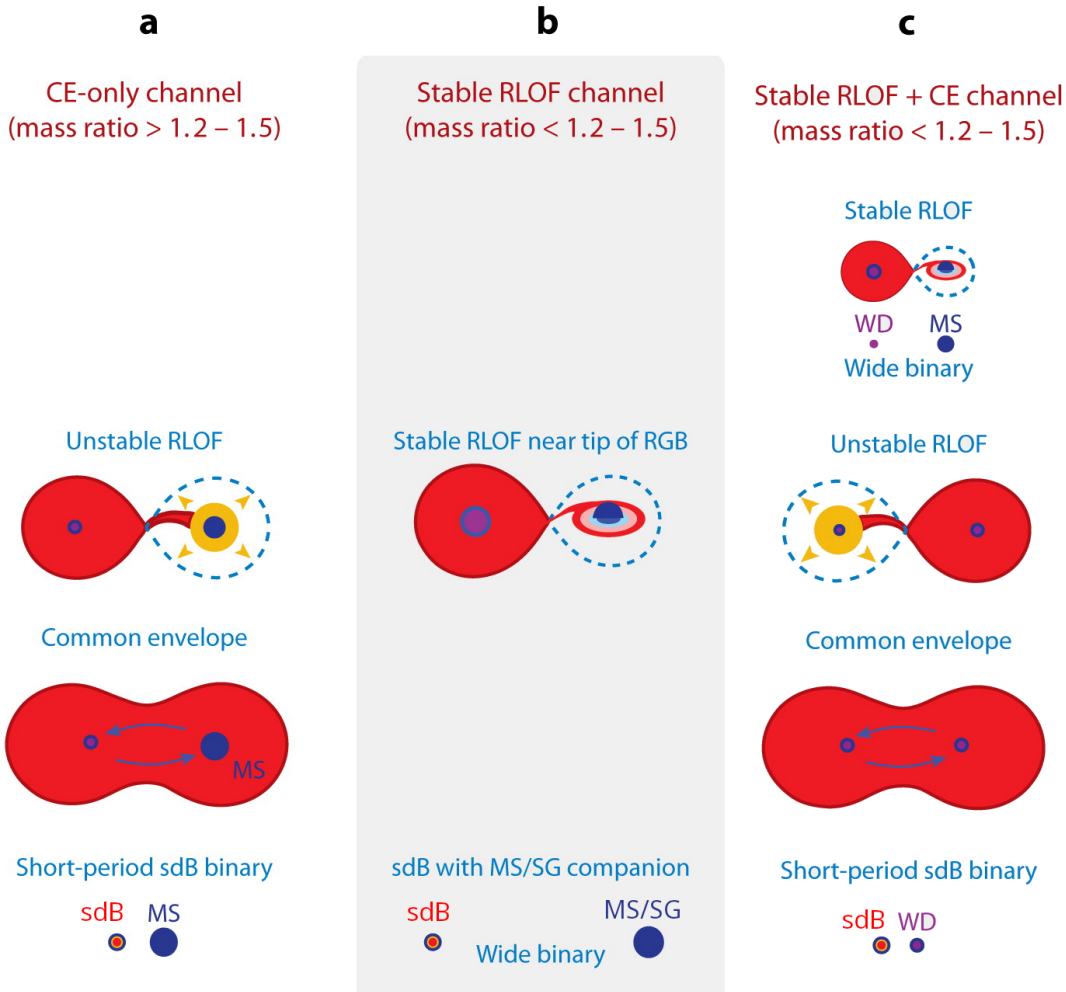


**Figure 1.2:** Different formation channels for sdBs in binary systems. **a)** An sdB is formed after dynamically unstable mass transfer (common envelope) during the RGB phase of the primary and when the companion is still a MS star, producing a close sdB + MS binary. **b)** The sdB star forms after stable RLOF is initiated close to the RGB when the companion is a MS or subgiant star. A wide sdB + MS/SG is formed. **c)** A first phase of mass transfer via stable RLOF forms a low-mass white dwarf, while the sdB star results from a second phase of mass transfer via common envelope. The result is a close white dwarf + sdB binary. This figure has been adapted from Heber (2009).

reduces the orbital distance. After ejecting the envelope, a close binary consisting of the core of the RGB star and the previously formed white dwarf is revealed. If the exposed core of the RGB star is massive enough to ignite helium, a close sdB with a white dwarf companion is formed. Otherwise, a close double white dwarf binary is formed.

---

iii) **The helium WD Merger:** This channel involves the merger of two helium white dwarf stars resulting in a single sdB star, unlike in the previously explained channels in which the newly sdB always has a binary companion (Webbink, 1984; Iben & Tutukov, 1986). In the pre-merger phase, the helium white dwarf binary system needs to be close enough for gravitational waves (Taylor et al., 1979) to rapidly shrink the orbit, causing the merger. Finally, the mass of the resulting helium white dwarf is enough to ignite helium, resulting in a single sdB.

In summary, depending on the type of mass transfer that gives rise to the sdB star, it will result in binary systems with different orbital periods. The stable Roche lobe overflow formation channel results in sdB stars with relatively long periods up to  $\sim 1800$  d based on the binary population synthesis models of Vos et al. (2020). These systems are called wide sdB binaries. On the other hand, for the common envelope formation channel, the significant inspiral during the common envelope phase results in systems with very short orbital periods (typically less than a few days Han et al. 2002). These systems are called close sdB binaries. In Figure 1.2, the left and right panels show the formation of short-period systems, which require a common envelope phase, while the middle panel shows the scheme for the formation of a long-period system via stable Roche lobe overflow. The helium WD merger channel will produce a single sdB star. In order to obtain two helium WD stars close enough to merge, at least one common envelope phase must have previously happened.

The range of masses for sdB stars also depends on the evolutionary path by which they are formed. Most studies of sdB stars assume a canonical mass of  $M_{\text{sdB}} \sim 0.47 M_{\odot}$ , which corresponds to the core mass for a  $\sim$ solar mass giant at the tip of the RGB, where the helium core flash occurs. However, the most accurate observational constraints of the masses reveal a rather broad mass range. For example, Fontaine et al. (2012) obtained an empirical range of  $M_{\text{sdB}} \sim 0.35 - 0.63 M_{\odot}$  from asteroseismology of 15 pulsating sdBs, and a somewhat broader range of  $M_{\text{sdB}} \sim 0.29 - 0.63 M_{\odot}$  if eclipsing sdB binaries are also included, as can be seen in Figure 1.3.

Theoretically, the range of possible masses for sdBs was calculated by Han et al. (2002), who showed that the resulting mass depends on the progenitor mass and other assumed parameters and physical processes, such as metallicity, core overshooting, etc. While the derived masses were restricted to a rather small range of  $M_{\text{sdB}} \sim 0.45 - 0.48 M_{\odot}$  (i.e. close to the canonical value) for low-mass progenitor with initial masses  $\lesssim 1.3 M_{\odot}$ , progenitors with larger initial masses can lead to smaller sdB masses (as low

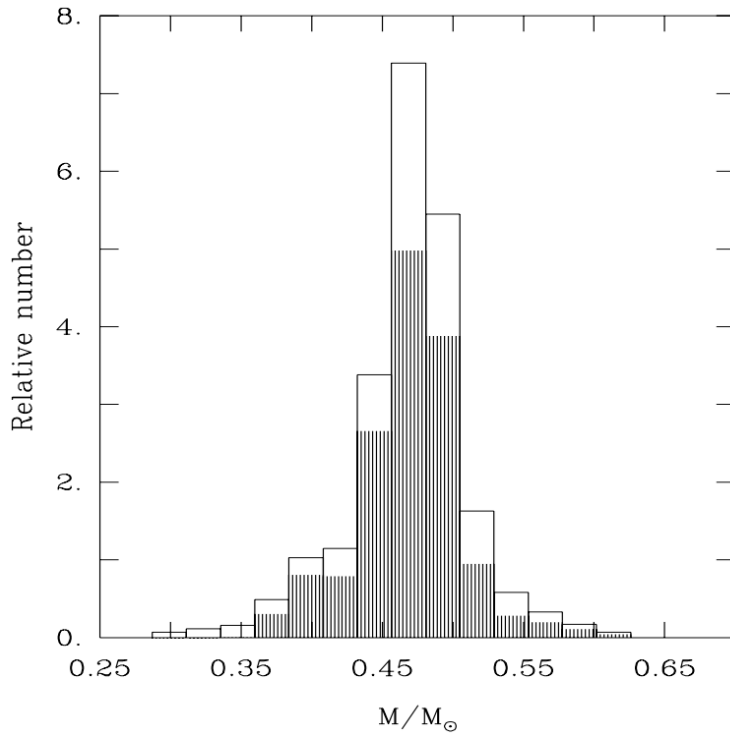


**Figure 1.3:** Figure taken from Fontaine et al. (2012) showing the empirical mass distribution of sdB stars with accurate mass estimations. The white histogram is based on a raw distribution for 22 sdB stars with accurate masses, including 15 pulsators and 7 eclipsing sdB binaries, obtained by adding together 22 Gaussians, each representing a measurement defined by a mass value and its associated  $1\sigma$  uncertainty. The shaded histogram is for the pulsators only.

as  $\sim 0.32 M_{\odot}$ ) but also to much larger masses if the progenitor was more massive than  $\sim 3 M_{\odot}$ .

Having accurate and reliable constraints of the sdB masses, both from an observational and theoretical point of view, is crucial to test the evolutionary paths towards these stars. The work from Han et al. (2002) was based on the stellar evolution code from Eggleton (1971). I here redo these calculations and refine the grids using the most updated and flexible open source code *Modules for Experiments in Stellar Astrophysics* (MESA, Paxton et al., 2011, 2013, 2015, 2018, 2019; Jermyn et al., 2023) to provide updated mass ranges for sdB stars depending on the mass and metallicity of the progenitor. I also study the effects of including core overshooting during the main sequence phase of the progenitors of the sdBs.

## CHAPTER 2

# Reviewing the work from Han et al. (2002)

In order for an sdB star to form, the envelope must be ejected close to the tip of the RGB, so that the core is massive enough to ignite helium after the envelope ejection. This leads to the question: how close to the tip of the RGB phase should the envelope be ejected in order to form an sdB star? We know that if this happens right on the tip of the RGB an sdB star will form. However, there is a range of radii when it is also possible to remove the envelope and still ignite helium such that an sdB is formed, which translates into a range of sdB masses. The pioneering work of finding this range was done by Han et al. (2002). In this work, they used two codes: an updated version of the Eggleton code (Eggleton, 1971, 1972, 1973), which is a detailed stellar evolution code that was used to determine the structure of the star and follow the evolution of the sdB, and a binary population synthesis (BPS) code (Han et al., 1995) used to examine different formation channels.

The Eggleton code includes the relation between mixing length and local pressure scale height  $\alpha = l/Hp$ . The value of  $\alpha$  is set to 2 based on a fit to the Sun (Pols et al., 1998). For convective overshooting, the code uses an approach based on stability criteria called the ' $\delta_{ov}$  prescription', where the condition for mixing to occur in a region is:

$$\nabla_{\text{rad}} > \nabla_{\text{ad}} - \frac{\delta_{\text{ov}}}{2.5 + 20\zeta + 16\zeta^2}, \quad (2.1)$$

where the constant  $\delta_{\text{ov}}$  is a free parameter introduced by Onno Pols for their overshooting model and  $\zeta$  is the ratio between the radiation pressure and the gas pressure. According to Schroder et al. (1997); Pols et al. (1997), the value that best fits the observed systems is  $\delta_{\text{ov}} = 0.12$ . This value corresponds to an overshooting length of  $\sim 0.25$  of the local pressure scale height. In Chapter 4 I will compare this prescription with the one used in my MESA models.

The BPS code is a Monte Carlo simulation code that uses a grid of stellar evolution models, which was previously obtained with the Eggleton code. Given a binary sample, the BPS code performs all necessary interpolations on the model grid, integrating mass loss along evolutionary trajectories for an assumed stellar wind law, and adjusting the orbital parameters considering binary interactions.

To carry out the evolution of the star, they used various physical parameters. However, they presented the results for three models: solar metallicity ( $Z=0.02$ ), no wind on the RGB and no overshooting; solar metallicity ( $Z=0.02$ ) with a Reimer's factor of  $\eta = 0.25$  for wind mass loss during the RGB phase and core overshooting during the main sequence; and the same as the later but for a lower metallicity ( $Z=0.004$ ).

The minimum and maximum sdB masses as a function of progenitor mass obtained by Han et al. (2002) are presented in Figure 2.1, for the solar metallicity models, with and without overshooting (black and blue lines, respectively). According to Han et al. (2002), the core mass at the tip of the RGB reaches a minimum for an initial mass of  $\sim 2.05 M_{\odot}$  (for the case with overshooting) which corresponds to the maximum initial mass that experiences a core helium flash. For more massive stars, the cores ignite helium under non-degenerate conditions. The authors did not give the results for massive stars without overshooting, however, we can still see from this Figure that the maximum initial mass for stars that develop a degenerate helium core is shifted towards smaller values when overshooting is included. These results agree with those obtained by Ostrowski et al. (2021), who studied the evolution of sdB stars using the predictive mixing and convective premixing schemes from MESA and showed the dependence of the core mass at the tip of RGB on different scales for core overshooting (their Figure C4).

It can also be observed in Figure 2.1 that the minimum core mass to ignite helium after losing the envelope remains nearly constant for initial masses between  $\sim 2.05$  and  $\sim 2.5 M_{\odot}$  and starts to increase steeply for more massive progenitors. Recently,

---

Scherbak & Fuller (2023) used a sample of close double white dwarf binaries in order to constrain common envelope evolution. In their Figure 7 they show the helium core mass as a function of progenitor mass during the RGB phase with MESA, highlighting the minimum core mass needed to produce an sdB star. A constant minimum core mass to form an sdB star was also obtained by these authors for stars that do not ignite helium degenerately<sup>1</sup>. However, they did not predict an increase of the minimum core mass for more massive progenitors. Comparing their Figure 7 with the results from Han et al. (2002) for the minimum sdB masses, it seems that the increase predicted by Han et al. (2002) comes from requiring that the star’s envelope is deeply convective. I will test this hypothesis in Section 2.1.

In the results obtained by Han et al. (2002) the effect of the wind is very small. That is, it does not affect the helium core. This can be inferred as the lines for the cases with core overshooting (which include Reimer’s wind mass loss with  $\eta = 0.25$ ) and without overshooting (where no mass loss was considered) coincide for masses less than  $\sim 1.3 M_{\odot}$ , which is when the core of the star is radiative and the effect of overshooting is negligible. Therefore, for this range of masses, the only process that could produce a variation in helium core is the wind, and this is not the case.

Another physical parameter studied by Han et al. (2002) was the metallicity. Figure 2.2 shows the comparison of the values they obtained for the models with overshooting for two different metallicities. As in Figure 2.1 the range of maximum and minimum values for the helium core to ignite after the envelope ejection is shown. The black lines are for stars with  $\sim$ solar metallicity ( $Z = 0.02$ ) and the purple lines are for stars with a lower metallicity ( $Z = 0.004$ ). Here we can see that for progenitor stars with low metallicity ( $Z = 0.004$ ) the whole range moves toward higher masses both for the tip and for the minimum helium core for an sdB star. In addition, for the lower metallicity case, the maximum initial mass for which the core becomes degenerate is smaller.

It is worth mentioning that the work carried out by Han et al. (2002) mentions the use of two codes (Eggleton and BPS) to carry out the evolution of stars up to the sdB phase. However Han et al. (2002) did not discuss in detail what methodology was used to find the minimum mass of the helium core that can form an sdB star in massive stars that do not develop a degenerate core. For example, it is not clear why the minimum sdB mass predicted by Han et al. (2002) increases for massive progenitors

---

<sup>1</sup>The models in this work do not contain overshooting, but I will show in the next chapter that my MESA models with overshooting also predict a constant minimum sdB mass for massive progenitors.

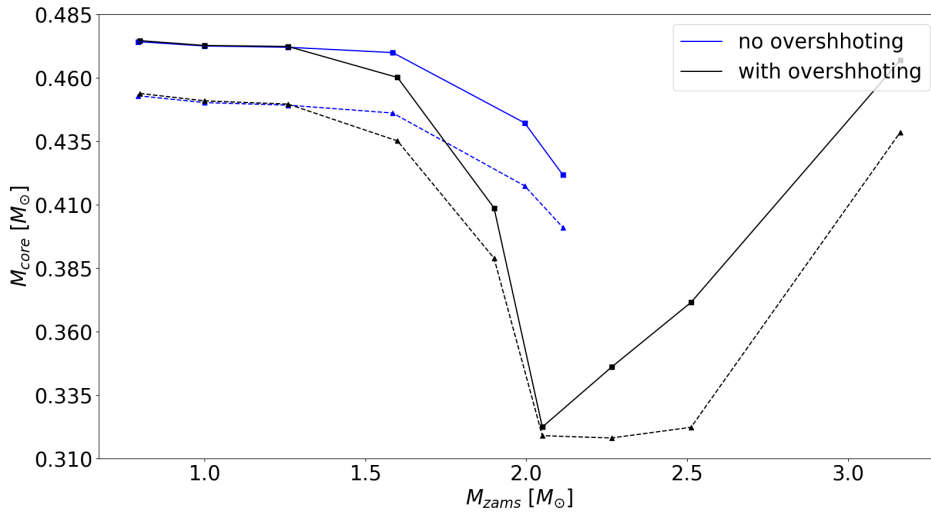


**Figure 2.1:** Mass range of sdB stars as a function of the initial mass from Han et al. (2002) for  $Z = 0.02$ . The black and blue lines represent the results with and without overshooting, respectively. The solid lines connect the squares that correspond to the maximum sdB masses, i.e. the helium core masses at the tip of the RGB. The dashed lines connect the triangles that correspond to the minimum core masses that can ignite helium after the envelope is lost.

while it remains constant in the MESA models from Scherbak & Fuller (2023).

## 2.1 Comparison with SSE

In order to better understand the results from Han et al. (2002), first, I compared their models with the results that can be obtained with a similar code, i.e. the single star evolution code (SSE) from Hurley et al. (2000). This code was used to obtain a first comparison given its ability to evolve many stars in a very short time because, in contrast to the detailed stellar evolution code MESA, the SSE code is based on fits to the stellar models. The models used for the fits in SSE are those from Pols et al. (1998), with a fixed overshooting parameter of  $\delta_{ov} = 0.12$ , meaning that overshooting cannot be changed or turned off in SSE.

A metallicity of  $z=0.02$  and a Reimer’s mass loss factor of  $\eta = 0.25$  were chosen to compare with the results of Han et al. (2002). SSE was used to compute the helium core mass at the tip of the RGB for different initial masses in the range of  $0.8 - 3.5 M_{\odot}$  in steps of  $0.01 M_{\odot}$ , which is a much finer grid than the one given by Han et al. (2002).

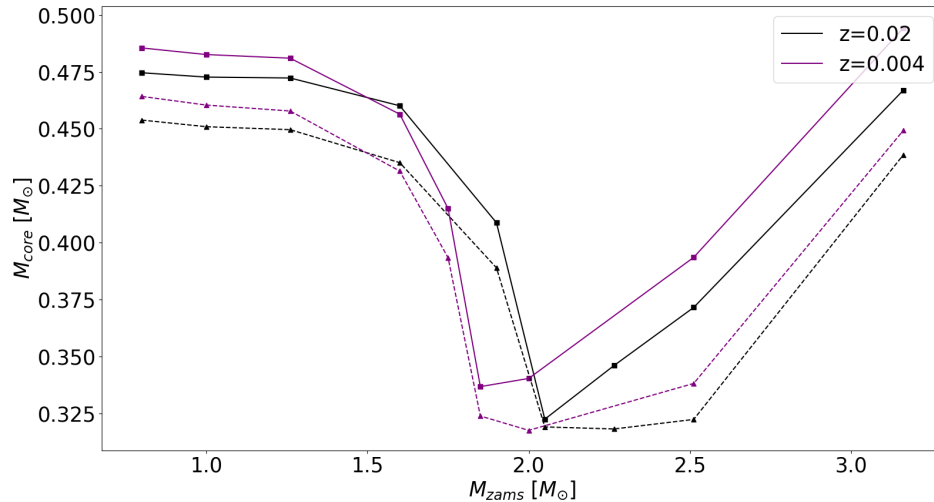


**Figure 2.2:** Mass range of sdB stars as a function of the initial mass from Han et al. (2002) for  $Z = 0.02$ ,  $Z = 0.004$  and a Reimer’s mass loss factor of  $\eta = 0.25$  during the RGB. The black and purple lines represent the results with  $Z = 0.02$  and  $Z = 0.004$ , respectively. The solid lines connect the squares that correspond to the maximum sdB masses, i.e. the helium core masses at the tip of the RGB. The dashed lines connect the triangles that correspond to the minimum core masses that can ignite helium after the envelope is lost.

However, the minimum core mass needed to produce an sdB star cannot be computed with SSE, so the core masses at the base of the subgiant and RGB phases were computed for comparison.

Figure 2.3 shows the comparison between the calculations performed with SSE and the results from Han et al. (2002). The helium core mass at the tip of the RGB is represented by the solid lines. The red line corresponds to the core masses obtained with SSE while the black and gray lines are for Han’s calculations with and without overshooting, respectively. From this comparison, it becomes evident that overshooting was treated in the same way in the calculations from Han’s as in the SSE code. The overall agreement between the two codes is surprisingly good, even though SSE is based on fits to stellar models, while the Eggleton code is a detailed evolution code. Small differences are obtained for stars that develop a partially degenerate core during the RGB, for which probably the fits used in SSE are not so accurate. The values also deviate for more massive stars which might be related to the fact that SSE fits are better for solar type stars.

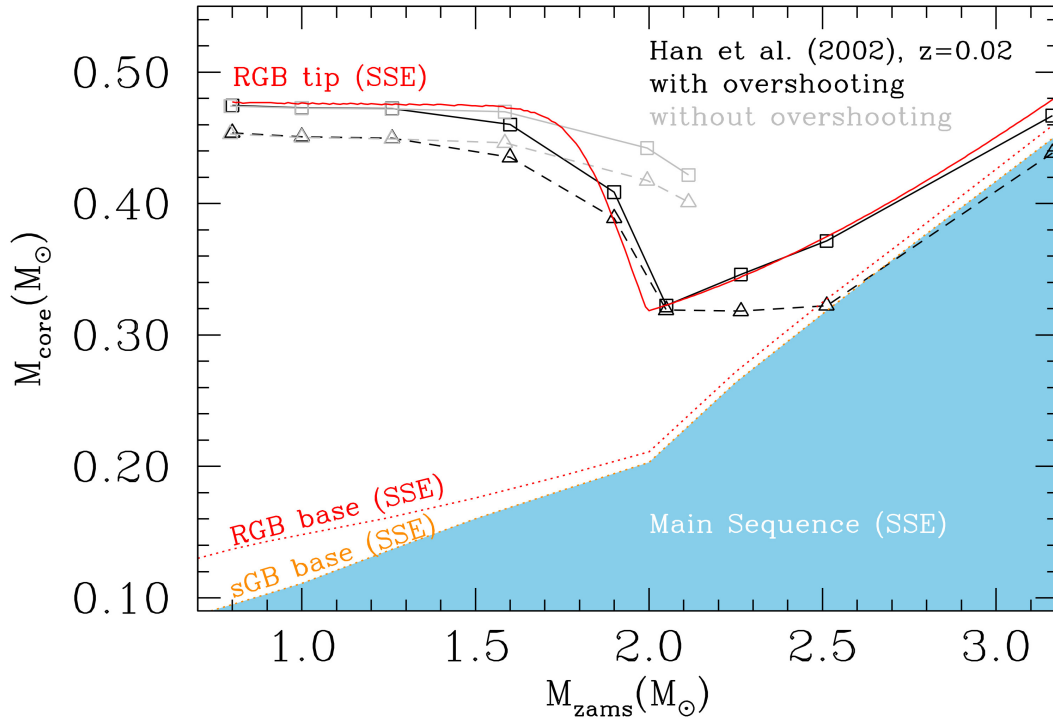


**Figure 2.3:** Core mass at different evolutionary phases as a function of initial mass for solar metallicity. The tip of the RGB is represented by the solid lines for the SSE calculations (red) and for Han’s calculations with (black) and without (gray) overshooting. The dashed black and gray lines correspond to the minimum sdB masses with and without overshooting, respectively, given by Han et al. (2002). Also shown as dotted lines are the core mass at the base of the red giant phase (red) and at the base of the subgiant phase (orange), below which the star is on the main sequence.

For stars initially more massive than  $\sim 2 M_{\odot}$ , where the core mass does not become degenerate during the RGB (according to the models with overshooting), the minimum core mass to ignite helium after the envelope ejection should remain constant (see e.g., Scherbak & Fuller, 2023). However, as mentioned before, Han et al. (2002) predicts an increase of this minimum core mass for stars with initial masses larger than  $\sim 2.5 M_{\text{sun}}$ . Looking at Figure 2.3, the minimum core mass predicted by Han et al. (2002) is very similar to the mass of the helium core at the base of the subgiant or RGB phases calculated with SSE (orange and red dotted lines, respectively). As we suspected, this was probably assumed by Han et al. (2002) since it is very unlikely that an sdB star is formed after mass transfer initiated from a main sequence star. In the common envelope scenario, a deep convective envelope is needed to ensure the

dynamically unstable mass transfer that produces the common envelope phase. In the case of stable mass transfer, as it was explained in the previous chapter (see also Figure 1.2), sdB progenitors should also be evolved stars on the RGB to ensure helium ignition in the core to occur when a small hydrogen envelope is left.

In the next chapter, I am therefore going to present the full range of possible core masses that can produce an sdB after the loss of the envelope according to the MESA simulations, but highlighting the progenitors that correspond to stars with a deep convective envelope.



## CHAPTER 3

# Models with MESA

In order to model the sdB stars, the stellar evolution code Modules for Experiments in Stellar Astrophysics (MESA, Paxton et al., 2011, 2013, 2015, 2018, 2019; Jermyn et al., 2023, r15140) was used. This code requires two initial parameters of the star, the initial mass and the metallicity. In addition, one has to adjust many other parameters in order to establish the physics inside the star in each of its evolutionary stages. In MESA it is possible to carry out the evolution of a single star and also the evolution of a binary system. The next logical thing would be to use the evolution of a binary system, but we want to reproduce the common envelope channel and, currently, MESA is not capable of solving this type of binary evolution. In order to reproduce the outcome of CE evolution channel, I used MESA to model a single star and artificially removed the envelope at the tip of the RGB, defined by the onset of helium burning in the core. In this way I obtain the canonical mass of an sdB, which corresponds to the maximum sdB mass for a given progenitor mass. In order to obtain the minimum mass for these stars, another part of the evolutionary process was to remove the envelope during the RGB phase but before the tip.

The modeling process can be divided into three steps. The first step is to evolve a star of a certain mass and metallicity from the pre-main-sequence phase to the terminal age main sequence (TAMS). During this step, it is important to consider overshooting on the core of the star during the main-sequence evolution. The second step is to evolve the star from the TAMS to the tip of the RGB. And the third step is to load the

star at different evolutionary stages within the RGB and rapidly remove the envelope, simulating the common envelope phase and evolve this naked star all the way to the cooling track.

### 3.1 From pre-MS to TAMS

This is the first evolutionary stage in my models where the initial mass and metallicity are defined. I have used a grid of initial masses from 0.8 to 6 solar masses and two different metallicities,  $Z = 0.02$  and  $0.004$ , following Han et al. (2002). Each star is evolved from the pre-main-sequence (pre-MS), where the star descends on the Hayashi track and is completely convective, until the end of the main sequence (TAMS), when hydrogen in the center of the star is depleted.

During the main sequence, the helium core is growing and, to establish the limit between the radiative and convective zones, the predictive mixing scheme is used. The algorithm looks for cells of material which are fully mixed, varying the distance above and below the boundary between two zones until the cell is fully mixed with the rest of the adjacent convection region. This mixing prescription involves re-evaluating opacities, densities, and other data throughout the mixed region. For a more detailed explanation see Paxton et al. (2018, Section 2.1) and Ostrowski et al. (2021). The mixing length alpha ( $\alpha_{MLT}$ ) is defined as the local pressure scale height and its typically used value is 1.8 (e.g., Ostrowski et al., 2021).

It is important to consider overshooting during this stage as the mass of the helium core at the end of the main sequence depends on mixing processes. The term overshoot refers to the transport of material and energy between the convective and radiative regions of the star. This creates a more realistic transition between the boundary of these two regions. There are three prescriptions for overshooting implemented in MESA: step overshooting, exponential diffusive overshooting, and extended exponential overshooting. For a detailed review of the three schemes see section 2 in Pedersen et al. (2018).

For my MESA models I adopted the exponential diffusive overshooting. In this prescription, overshooting is treated as a diffusion process with an exponentially decreasing diffusion coefficient (see, e.g., Zhang et al., 2022) which can be written as:

$$D = CD_0 \left( \frac{P}{P_{cz}} \right)^\theta, \quad (3.1)$$

where  $C$  and  $\theta$  are dimensionless model parameters,  $P$  is the pressure,  $P_{cz}$  is the value at the convective core boundary, and  $D_0$  is the diffusion coefficient in the convective core close to the convective boundary which is proportional to the mixing length ( $D_0 \sim l = \alpha H_p$ ). On the other hand, the overshooting diffusion coefficient formula adopted by the MESA code (Herwig, 2000; Paxton et al., 2011) is:

$$D = D_0 \exp\left(-\frac{2\Delta r}{f_{ov}H_p}\right), \quad (3.2)$$

where  $\Delta r = |r - r_{cz}|$  is the distance of the overshoot into the radiative layer and  $H_p$  is the local pressure scale height. As demonstrated by Zhang et al. (2022), assuming  $f_{ov} \ll 1$  one can approximate:

$$\exp\left(-\frac{2\Delta r}{f_{ov}H_p}\right) \approx \exp\left(-\frac{2}{f_{ov}} \int_{r_{cz}}^r \frac{dr}{H_p}\right) = \exp\left(-\frac{2}{f_{ov}} \ln \frac{P}{P_{cz}}\right) = \left(\frac{P}{P_{cz}}\right)^{\frac{2}{f_{ov}}}. \quad (3.3)$$

Using this approximation in Equation 3.2 and equating with 3.1 we obtain:

$$CD_0 \left(\frac{P}{P_{cz}}\right)^\theta = D_0 \left(\frac{P}{P_{cz}}\right)^{\frac{2}{f_{ov}}} \quad (3.4)$$

Considering  $C = 1$  (Herwig, 2000) it can be seen that  $f_{ov}$  is a dimensionless parameter related to  $\theta$  by  $f_{ov} = 2/\theta$ .

In MESA the free parameter  $f_{ov}$  sets the extent of the overshoot region and needs to be set by the user. I here adopted the recommended value from (Herwig, 2000),  $f_{ov} = 0.016$ , based on fits to the stellar models from Schaller et al. (1992), which is roughly equivalent to  $f_{ov,step} = 0.2$  in the step overshoot scheme.

For the models in this work, the exponential diffusive overshoot scheme is used during the main sequence evolution between the core and the envelope of the star. To set how far from the convective boundary overshooting actually starts, a parameter  $f_0$  needs also to be set, which defines the distance below the boundary where overshooting starts. I used  $f_0 = f_{ov}/2 = 0.008$  which implies that the same distance is considered towards the core and towards the envelope. Finally, MESA allows one to define a range of star masses over which overshooting is gradually enabled. I defined this range to be  $1.1 - 1.3 M_\odot$  which means that no overshooting is considered below  $1.1 M_\odot$  (where a star has a radiative core) and is fully established above  $1.3 M_\odot$ .

An example of an inlist file for this first evolutionary phase can be found in A.1

## 3.2 From TAMS to the tip of the RGB

At the end of the main sequence, hydrogen is depleted in the center and the star moves towards the subgiant branch, where a shell of hydrogen burning is still active around the contracting core, adding helium ashes to the layers below. Once the core reaches the Schönberg–Chandrasekhar limit, it begins to contract more rapidly, releasing gravitational energy which causes an expansion of the envelope. The hydrogen burning shell narrows but its temperature and density increase, rising the energy generation rate, which causes a larger expansion of the envelope. Convection is established on the surface of the star because of the drop in the temperature. Once the stellar envelope becomes deeply convective it begins its ascend on the HR diagram on the RGB phase. Whether the helium core becomes degenerate or not during the RGB will depend on the initial mass of the star and the inclusion or not of core overshooting during the main sequence. I will discuss this in more detail in Section 3.5.1. The expansion of the outer layers can cause mass loss, especially when the star expands closer to the tip of the RGB. Given the similarity of the results presented by Han et al. (2002) for their models with and without mass loss (see Chapter 2), only models with mass loss were simulated with MESA. In order to be consistent with most of the models from Han et al. (2002), I have used a Reimer’s wind loss factor of  $\eta = 0.25$ .

To stop the simulation just at the tip of the RGB, the total power of the helium burning reactions was used, with the limiting value set to  $10 L_{\odot}$ . From here, the mass of the helium core at the tip of the RGB is obtained, which is considered as the maximum mass for an sdB star with a given initial mass. For the minimum sdB mass the models should be stopped before reaching the tip of the RGB. This is obtained simply by stopping the simulation at a specific model number which corresponds to a helium core mass smaller than the core mass at the tip of the RGB. Whether this core mass ignites helium after removing the envelope is tested in the third step of my modelling process.

An example of an inlist file for this second step can be found in A.2.

## 3.3 Removing the envelope during the RGB phase and evolving until the white dwarf cooling track

Once the model has reached the mass of the helium core I was looking for, either at or near the tip of the RGB, the next step was to quickly remove the hydrogen envelope

from the star emulating a common envelope phase. While some studies simulating sdB stars with MESA used an extreme wind (e.g.,  $10^{-3} M_{\odot}/\text{year}$ ) to remove the envelope (Krtićka et al., 2016; Xiong et al., 2017), more recent work (e.g., Schindler et al., 2015; Ghasemi et al., 2017; Vos et al., 2019) used a built-in tool called ‘Relax Mass’. For the latter, which is the one I chose, one needs to set two parameters: the final mass of the star and how fast the envelope will be removed. Regarding the final mass, I wanted to leave a small hydrogen envelope around the helium core, part of which was incorporated into the core after removing the envelope and before helium ignition. I found that leaving a hydrogen envelope of  $0.01 M_{\odot}$  for the ‘Relax Mass’ process, considered as the upper limit for sdBs (e.g., Heber, 2016), resulted in a hydrogen envelope mass around the sdBs of the order of  $\sim 10^{-2} - 5 \times 10^{-4} M_{\odot}$  during the sdB phase, consistent with the work from Schindler et al. (2015). So, for example, if the loaded model has a helium core mass of  $0.435 M_{\odot}$ , the input parameter (final mass) was set to  $0.445 M_{\odot}$ . The second parameter establishes the maximum mass-loss rate allowed in this process for which I used an option that implies that MESA will decide the most optimal mass-loss ratio.

From this point, having already removed the envelope, the star evolves towards the extreme hot end of the horizontal branch, where the sdB phase begins. The evolution is terminated when the luminosity of the star drops below  $\log(L/L_{\odot}) = -3.5$ . At this stage the star is already on the white dwarf cooling track, thus reaching the region of the white dwarf stars in the HR diagram (see Figure 1.1)

Again, I included an example of an inlist file for this step in the appendix A.3.

### 3.4 Finding the minimum sdB masses

As I have already mentioned before, the main objective of this work is to find the mass range for sdB stars using MESA. To search for the minimum mass an sdB star can have, in addition to looking at models with a helium core mass which is less than the one at the tip of the RGB, we must check whether the code has managed to reproduce an sdB star, i.e. if helium was ignited in the core. My first approach was to search for the lowest core mass that did not become a white dwarf after removing the envelope, for each initial mass. However, low-mass stars models with degenerate core, did not manage to ignite helium, as the code was not capable to solve the helium core flash in a naked star. Due to numerical issues when the model was trying to converge during this phase, the timestep was reduced with each iteration reaching

the minimum timestep limit ( $< 10^{-20}$  seconds).

After researching for around two months I finally found that to resolve this error it was necessary to include the following key parameter in the input file:

```
convergence_ignore_equL_residuals = .true.
```

By including this, MESA relaxes some of the very strict convergence controls related to energy conservation.

After including this parameter the code was able to resolve the helium core flash and continue the evolution, becoming an sdB star. In this way, I was able to verify that the model with the lowest core mass that previously presented an error was precisely the one that corresponds to the minimum core mass that ignited helium. To evaluate whether a model has succeeded to burn helium in a stable way, i.e. going through the sdB phase, I looked at the mass of the carbon core. If the model had a final carbon core mass larger than 0 it was assumed that it experienced a phase of core helium burning as an sdB star. Otherwise, it was considered a helium white dwarf.

Initially, I applied the ‘Relax Mass’ process loading models on the RGB with increasing core masses, in steps of  $0.01 M_{\odot}$ , until I found a model that went through the sdB phase. Later I used finer steps of  $0.001 M_{\odot}$  within this core mass and the previous model, that did not create an sdB star, in order to get an accurate minimum sdB mass.

In the next section I present the results obtained using the method just described for the modelling process.

## 3.5 Results

With the method described in the previous Section, it was possible to model sdB stars with MESA. Figure 3.1 shows the evolution in the HR diagram for a star with an initial mass of  $1.5 M_{\odot}$ , solar metallicity and including core-overshooting during the main sequence phase. The left panel shows the evolution when the envelope was artificially removed at the tip of the RGB phase, which results in the maximum sdB mass for this initial mass. In the right panel, on the other hand, the envelope was removed when the core mass was the minimum needed to ignite helium after losing the envelope, leading to the minimum sdB mass for a  $1.5 M_{\odot}$  progenitor. The gray dotted lines show the whole evolution, while the black and red dots correspond to steps of 1 Myr, with the red dots highlighting the sdB phase.

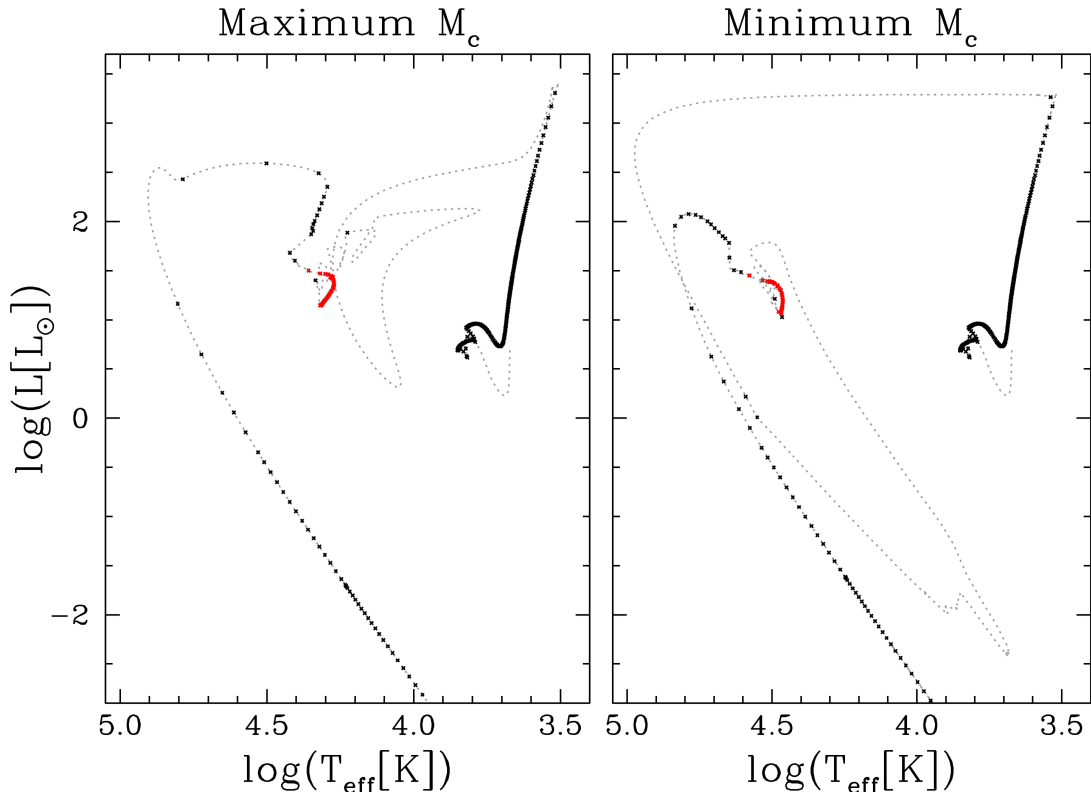


**Figure 3.1:** HR diagram evolution for a  $1.5M_{\odot}$  star where the envelope was artificially removed either at the tip of the RGB (*left*) or when the core mass on the RGB corresponds to the minimum mass that ignites helium after the envelope is ejected (*right*). The gray dotted lines show the whole evolution while the black and red dots are in steps of 1 Myr with the sdB phase highlighted as red dots.

We can see that by removing the envelope at the tip of the RGB the star manages to ignite the helium core very quickly (after only  $\sim 17\,000$  yr), because the necessary conditions for pressure and temperature were already almost reached. On the other hand, for the minimum mass, the star first needs to contract to reach the necessary conditions to ignite helium. This can be seen in the right panel of Figure 3.1, where the star first goes towards the white dwarf cooling track until enough compression is achieved and helium can be ignited (after  $\sim 2.8$  Myr) moving the star back up in the HR diagram to become an sdB.

The sdB phase was identified due to the presence of a convective core after the removal of the envelope. In Fig 3.2, I show the evolution of the luminosity (top), effective temperature (second panel from top), radius (third panel from top) and location of the convective region (bottom) after the envelope was removed for the  $1.5M_{\odot}$  star

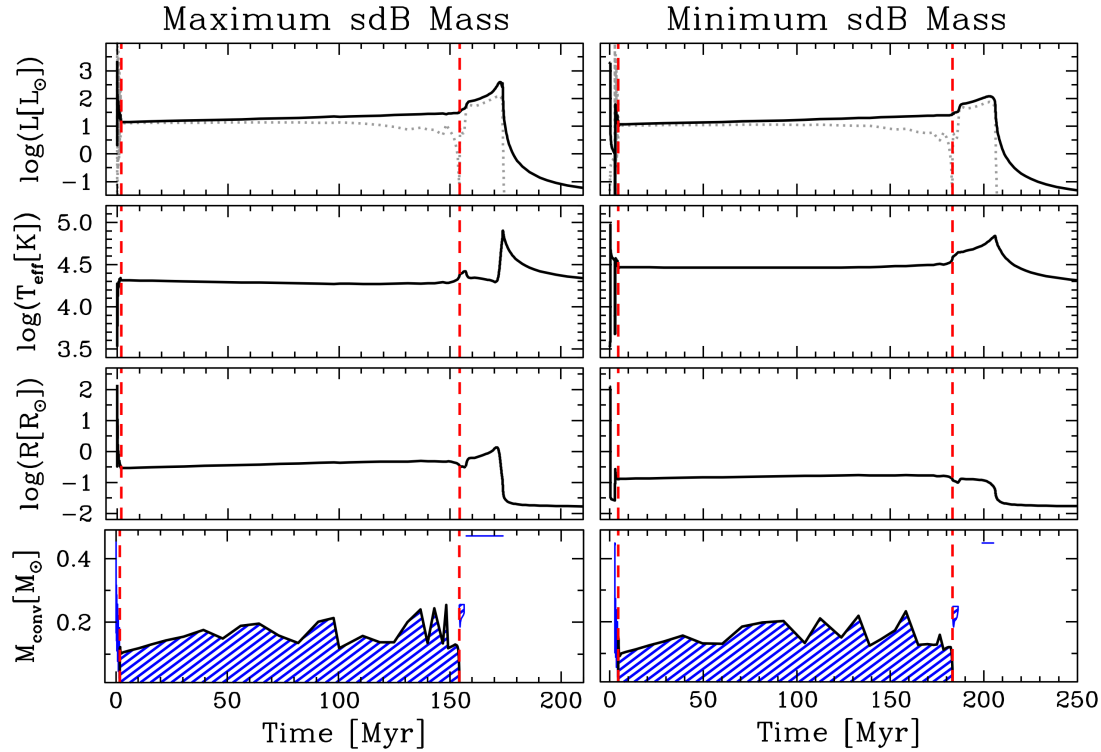


**Figure 3.2:** Evolution of the total (black solid line) and helium (dotted gray line) luminosity (*top*), effective temperature (*second panel from top*), radius (*third panel from top*) and location of the largest convective region (*bottom*) for a  $1.5 M_{\odot}$  star after removing the envelope at the tip of the RGB (*left panel*) or when the core mass on the RGB corresponds to the minimum mass that ignites helium after the envelope is ejected (*right panel*). In the bottom panel, the black line represents the mass of the convective core while the blue dashed regions show the location of the largest convective zone. The dashed red lines indicate the beginning and end of the sdB phase. The time was set to 0 after the envelope was fully removed to facilitate the visualization of the duration of the sdB phase

either at the tip of the RGB (left panel) or when the core mass corresponds to the minimum mass that ignites helium after the envelope is ejected (right panel). In the top panels, the dotted gray lines show the power of helium burning (as the logarithm of the total thermal power from triple-alpha process, excluding neutrinos, in solar luminosities). The blue dashed regions in the bottom panel show the location of the largest convective zones while the black line represents the convective core mass. The two red dashed vertical lines indicate the beginning and end of the sdB phase, which last  $\sim 150$  Myr and  $\sim 180$  Myr, respectively. Both the mass of the convective core as well as the duration of the sdB phase are consistent with the results obtained by Ostrowski

et al. (2021, their Fig. 6). They found that for an initial mass of  $1.0 M_{\odot}$ , and using the predicting mixing scheme, the duration of the sdB phase was 147.9 Myr when the envelope was removed at the tip of the RGB.

One can see from Fig. 3.2 that the sdB that descends from the tip of the RGB phase (left panel) has a larger radius and a lower effective temperature, compared to the sdB with the minimum mass (right panel) for a  $1.5 M_{\odot}$  progenitor. This is a consequence of the hydrogen envelope that remains during the sdB phase. Although in both cases I left the same hydrogen envelope of  $0.01 M_{\odot}$  around the helium-core during the ‘Relax Mass’ process, the sdB that descends from the tip of the RGB ignites helium very quickly (only  $\sim 17\,000$  yr after the envelope removal), while hydrogen was still being burned and incorporated into the core. The ignition of helium halts the burning of hydrogen and results in an sdB with a larger hydrogen envelope (of  $\sim 9 \times 10^{-3} M_{\odot}$ ). On the other hand, for the model with the minimum sdB mass, the hydrogen burning phase lasts for  $\sim 140\,000$  yr after the envelope removal, while ignition of helium occurs  $\sim 2.8$  Myr after removing the envelope, when the star was already a white dwarf and the hydrogen envelope was smaller ( $\sim 5 \times 10^{-4} M_{\odot}$  for this model).

It can also be seen from Figure 3.2 that after the end of the sdB phase, when helium core burning stops, the whole star experiences a rapid contraction phase, decreasing the radius while increasing the luminosity and effective temperature. The power of helium burning quickly recovers (see dotted gray line in the top panels), increasing the luminosity, due to the ignition of helium in a shell around the inert core (small convective zone just after the end of the sdB phase in the bottom panels). The behaviour of the radius and effective temperature during the shell helium burning phase is very different for the two models. For the maximum sdB mass, the radius increases causing the effective temperature to decrease slightly. The star moves up and slightly to the right on the HR diagram while it stays in the same temperature range of a B-type star, due to the thicker hydrogen envelope. On the other hand, for the minimum sdB mass, the radius decreases slightly and the effective temperature increases, moving the star up and to the left on the HR diagram, ascending towards the phase where hot subdwarf O (sdO) stars reside. During the helium shell burning phase, part of the remaining hydrogen envelope is burnt and converted to helium (marked as a nearly horizontal blue line in the bottom panels), leading to very similar hydrogen envelope masses ( $\sim 4 \times 10^{-4} M_{\odot}$ ) for the resulting white dwarfs in both cases. However, given that there was a larger hydrogen envelope around the more massive sdB, a peak in the luminosity and a rapid increase in effective temperature, associated with hydro-

gen shell burning, is observed in the left panel just before entering the white dwarf cooling track.

I note that the differences just outlined for the two sdBs, with the maximum and minimum sdB mass for a  $1.5 M_{\odot}$  progenitor, are a direct consequence of having left the same envelope mass after the envelope removal, which might not be realistic. It might well be that removing the envelope closer to the tip of the RGB is more efficient, given the lower binding energy of a more extended envelope. This might translate into an initially smaller hydrogen envelope around the core compared to the case in which the envelope is ejected earlier on the star's evolution. Therefore, one should not conclude from these results that sdBs descending from more evolved progenitors are colder and larger due to their larger hydrogen envelope, or that they do not pass through the location of sdO stars during the shell helium burning phase. Given that the detail mechanism of the mass loss to form an sdB is not entirely understood, the mass of hydrogen that remains around the helium core after removing the envelope is unknown, albeit it should be small. As I mentioned earlier, I have chosen to leave  $0.01 M_{\odot}$  following the work of Schindler et al. (2015).

For the two examples presented in Figs. 3.1-3.3, given the small envelope left, the stars fail to reach the asymptotic giant branch. The post-sdB phase, with shell helium burning, lasts for  $\sim 10 - 20$  Myr, after which the power of helium burning drops dramatically, considerably decreasing the luminosity, effective temperature and radius, following the cooling track of a carbon/oxygen or a hybrid helium/carbon/oxygen white dwarf (see, e.g., Zenati et al., 2019, for a discussion on the formation of hybrid white dwarfs). The formation of hybrid white dwarfs with helium shells larger than  $0.01 M_{\odot}$  are of crucial interest for modelling the transient resulting from merging white dwarf binaries (Perets et al., 2019).

Given the mass of the initial star in this sample, helium is ignited under degenerate conditions in a series of rapid helium flashes that cause the loops in the luminosity and effective temperature seen in the left panel of Figure 3.1 just before the sdB phase. This is a very short phase which cannot be appreciated in Figure 3.2. Therefore, in Figure 3.3 I show the same four panels as in Fig 3.2 but focusing on the first few Myr after removing the envelope, to see the behaviour of important stellar parameters during the helium flashes. From the bottom panel of this figure, it can be observed that the ignition of helium starts off center, generating a series of flashes and the development of a convective zone that move towards the center of the star with each subsequent flash. Each of these flashes causes a contraction of the whole star and a drop in luminosity,

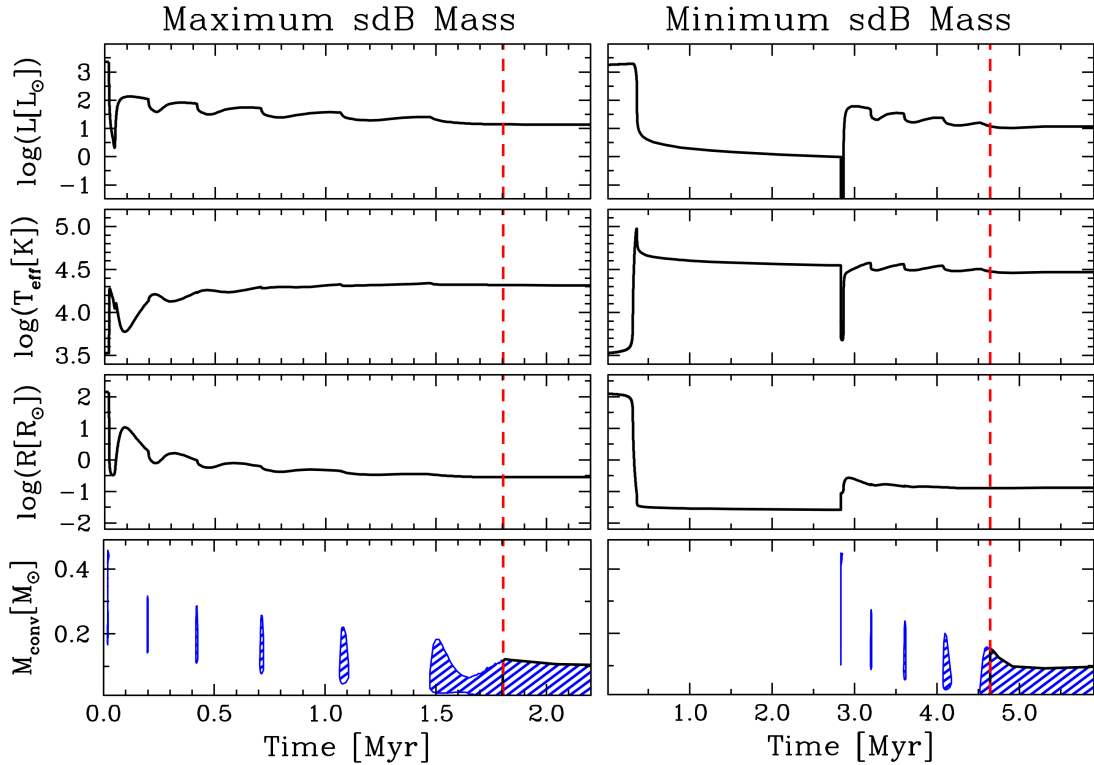


**Figure 3.3:** Same as in Fig. 3.2 but for the first few Myr after the envelope ejection, to focus on the phase of helium flashes, where the convection region is approaching the center with each flash. The red dashed line indicates the time when convection reaches the center, setting the beginning of the sdB phase.

while the effective temperature increases. The only exception is for the first flash in the model with the minimum sdB mass (right panel), because the star was already a white dwarf when the first flash occurred, and helium ignition resulted in an increase in radius and luminosity, and a decrease in effective temperature. The effect of the flashes on the surface are more evident for the first and more external flash, while the subsequent ones are progressively less intense, closer to the center, of longer duration and with less effect on the surface of the star. For this particular case, ignition of helium reaches the center during the sixth flash for the sdB with the maximum mass (left panel) and during the fifth flash for the sdB with the minimum mass (right panel), setting the beginning of the sdB phase (vertical red dotted line) when a convective core appears. These results are also strongly consistent with those obtained by Ostrowski et al. (2021, their Fig. C1) for a  $1 M_{\odot}$  star after removing the envelope at the tip of the RGB.

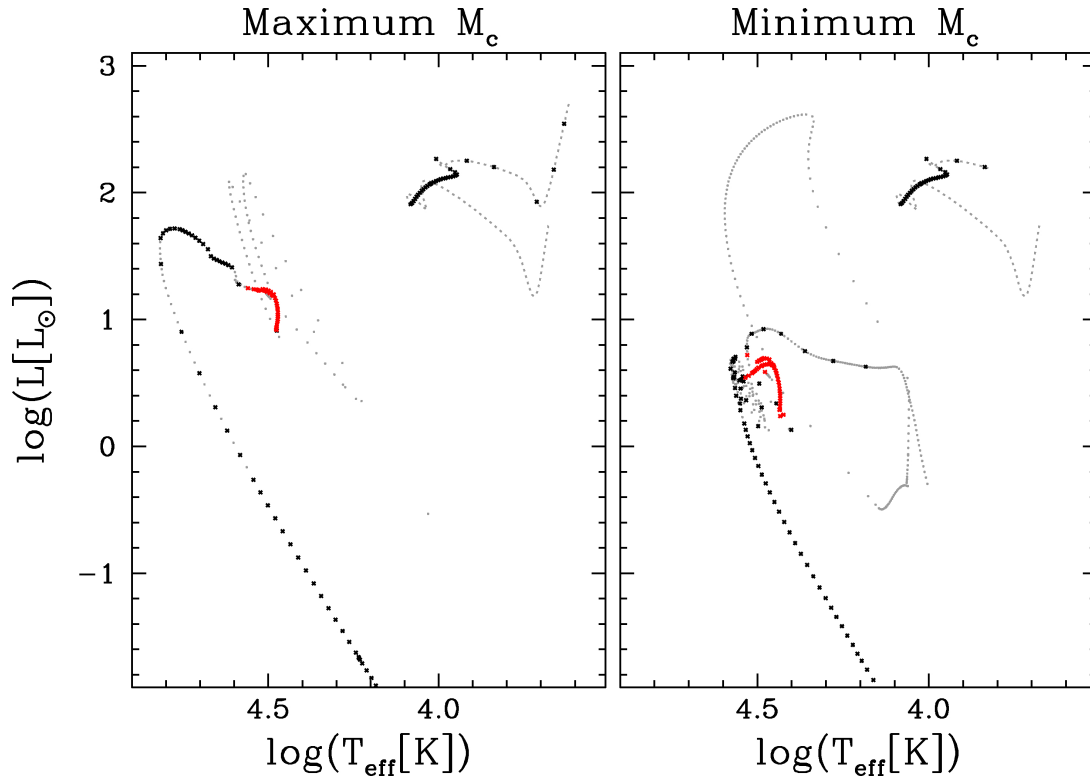


**Figure 3.4:** Same as in Figure 3.1 but for an initial mass of  $3 M_{\odot}$ .

For more massive stars, the helium core does not become degenerate during the RGB phase, and it, therefore, ignites smoothly. Figure 3.4 shows an example of the evolution in the HR diagram for a star with an initial mass of  $3 M_{\odot}$ . As in Figure 3.1, the left panel corresponds to the evolution if the envelope is removed at the tip of the RGB phase, while the right panel shows the evolution for the minimum core mass that managed to ignite helium and become an sdB star after removing the envelope. While the evolution for the sdB that was formed from a progenitor at the tip of the RGB goes somewhat smoothly, the evolution of an sdB formed when the stripped RGB star has the minimum helium-core mass to form an sdB shows a more erratic behaviour. The biggest difference is that the latter experiences late helium shell flashes after the sdB phase.

Having successfully reproduced the sdB phase with MESA, I can now present and analyze the results obtained for the maximum and minimum sdB masses depending on the initial mass, metallicity and overshooting.

### 3.5.1 SdB masses for solar metallicity ( $Z = 0.02$ )

First of all, I will focus on the case of solar metallicity ( $Z = 0.02$ ). The easier results to derive were the masses of the helium core at the tip of the RGB. Figure 3.5 compares the results with and without overshooting. The observed behavior is the same as that obtained by Ostrowski et al. (2021), that is, the maximum initial mass for which the core becomes degenerate during the RGB is smaller when overshooting is included.

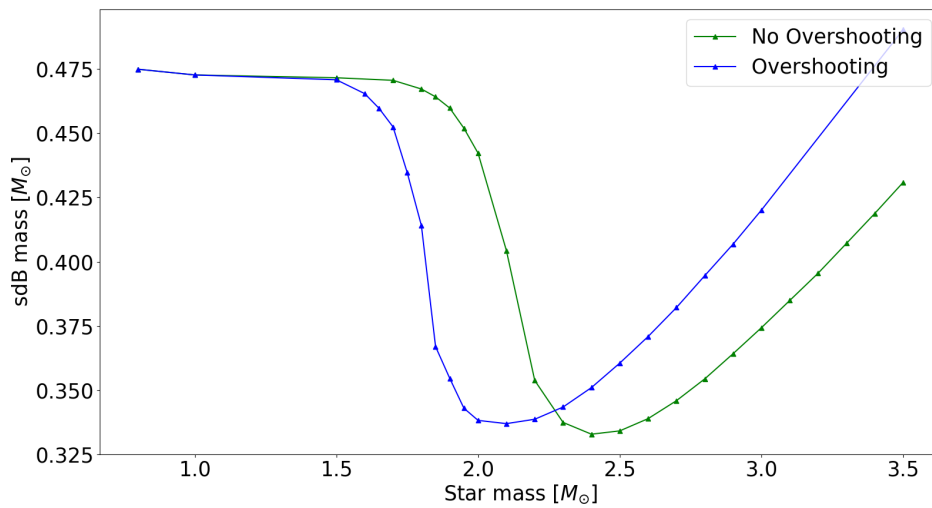


**Figure 3.5:** Maximum sdB mass as a function of initial mass for the MESA models with  $Z = 0.02$ , with (blue) and without (green) overshooting.

For the range of sdB masses, I will first analyze the behavior for models without overshooting. Figure 3.6 shows the minimum and maximum sdB masses as a function of initial mass. The maxima are represented by the darker green line connecting the calculated values (triangles). This corresponds to the mass of the helium core at the tip of the RGB plus the  $0.01 M_{\odot}$  hydrogen envelope left (much of which is burnt after the ‘Relax Mass’ process, as I explained in the previous Chapter). For stars with initial masses between  $0.8$  and  $1.6 M_{\odot}$  the maximum sdB mass is very close to the canonical value of  $\sim 0.47 M_{\odot}$ . From  $\sim 1.6 M_{\odot}$  the sdB mass decreases rapidly with increasing the initial mass, reaching a minimum value of  $0.33 M_{\odot}$  for an initial mass of  $2.4 M_{\odot}$ , and increases again for more massive progenitors.

The light green solid line in Figure 3.6 connects the results obtained for the minimum sdB mass using the procedure described Section 3.4. Given the large computa-

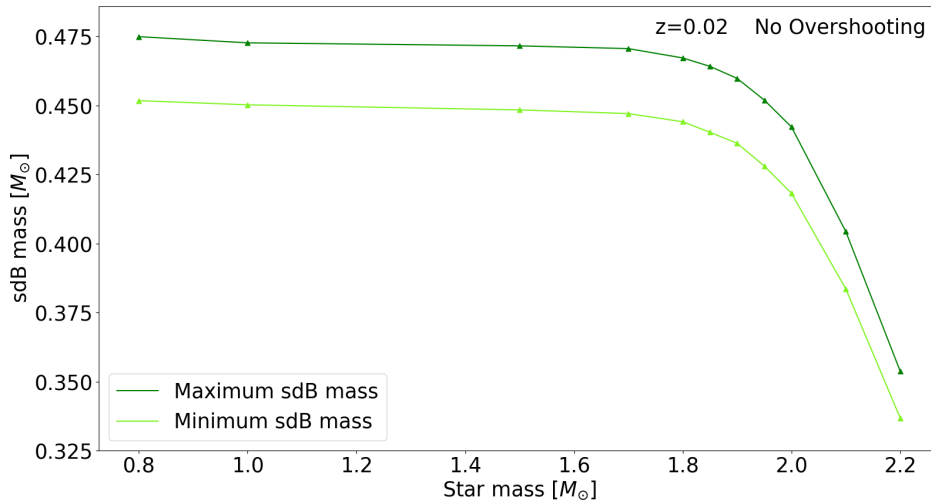


**Figure 3.6:** Minimum (darker green) and maximum (light green) sdB mass as a function of the initial mass from the MESA models with  $z = 0.02$  and without overshooting.

tional time required to obtain the minimum masses, I have only calculated them for initial masses up to  $2.2 M_{\odot}$ . This is because models without overshooting are not considered the most realistic, at least for stars above  $\sim 2 M_{\odot}$  (e.g., Constantino & Baraffe, 2018). I calculated the minimum sdB masses for this model only to be able to compare with the results of Han et al. (2002), who did not give the results without overshooting above  $\sim 2.3 M_{\odot}$ . The behavior of this curve is very similar to that obtained for the maximum mass. A nearly constant range of sdB masses between  $\sim 0.45$  and  $\sim 0.475 M_{\odot}$  is obtained for a rather broad initial mass range (between  $\sim 0.8$  and  $\sim 1.6 M_{\odot}$ ). However, the range of sdB masses is shifted towards smaller values for more massive progenitors.

For the solar metallicity model where overshooting was included, the results are presented in Figure 3.7. The blue and light blue triangles correspond to the maximum and minimum sdB masses, respectively, calculated with MESA. In this case, progenitors with initial masses up to  $6 M_{\odot}$  were considered for both the minimum and maximum sdB masses. However, in Figure 3.7 I only show the results up to  $\sim 4.5 M_{\odot}$ , since the data follow the same linear trend above. The general behavior is the same as for the case without overshooting. However, as the maximum initial mass for which the core becomes degenerate during the RGB is smaller for the models that include overshooting, both the maximum and minimum sdB masses start to drop towards

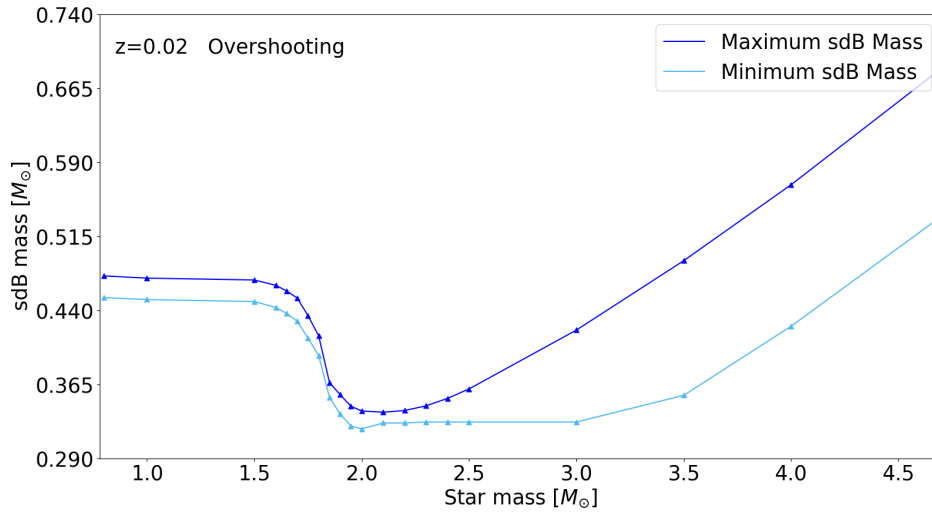


**Figure 3.7:** Same as in Figure 3.6 but for the model with overshooting.

smaller values at an initial mass of  $\sim 1.5 M_{\odot}$ , reaching a minimum at  $\sim 2 M_{\odot}$  where the maximum sdB mass is  $\sim 0.34 M_{\odot}$ . From  $2.1 M_{\odot}$  the maximum sdB mass starts to grow again, while the minimum sdB mass remains constant at  $0.327 M_{\odot}$ , at least for initial masses up to  $3 M_{\odot}$ , which is consistent with the results from Scherbak & Fuller (2023). For larger initial masses, however, the helium core mass at the TAMS is already larger than this value and helium was ignited for any core mass I chose after the TAMS to remove the envelope. It is highly unlikely that an sdB star can result if the envelope is removed during the MS, as there is still hydrogen in the core. Therefore, the minimum sdB mass was set to the helium-core mass at the TAMS plus the  $0.01 M_{\odot}$  of hydrogen envelope left, i.e. the first model at the base of the subgiant branch.

Even though sdBs can be produced from massive progenitors if they lose their envelope at the base of the subgiant branch, it is more likely for a mass transfer process to become dynamically unstable, and enter a common envelope phase, if the donor fills its Roche lobe when the envelope is already deeply convective, i.e. during the RGB phase. Therefore, I decided also to show the minimum sdB mass that is obtained for massive progenitors at the base of the RGB phase. MESA does not distinguish the different evolutionary phases. However, the base of the RGB can be defined assuming that a certain percentage of the envelope is already convective. Here I used the definition for the base of the RGB from the SSE code (see Section 2.1), i.e. when  $1/3$  of the envelope is convective.

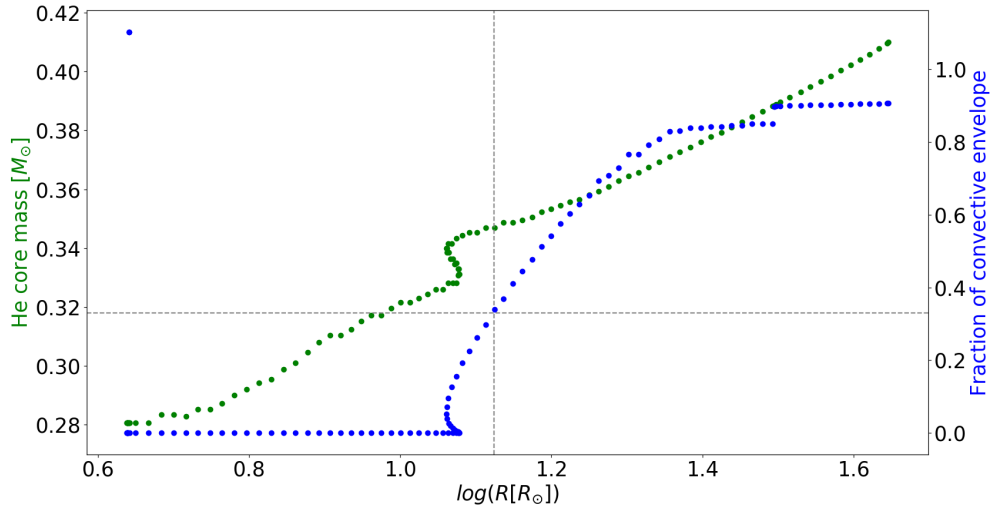


**Figure 3.8:** Helium core mass (green) and the fraction of the envelope that is convective (blue) as a function of the radius of the star from the TAMS to tip of the RGB for an initial mass of  $3 M_{\odot}$ . The horizontal gray dotted line marks where 33% of the envelope is convective, while the vertical gray dotted line indicates the value of the radius at which this occurs, from which the helium core mass at this point can be obtained.

An example of how the base of the RGB was obtained is shown in Figure 3.8 for an initial mass of  $3 M_{\odot}$  and solar metallicity evolved with MESA. The green points represent the values of the helium core mass as a function of the stellar radius as the star evolves from the TAMS to the tip of the RGB, while the blue dots represent the percentage of the envelope that is convective during this stage. The first evolution after the TAMS corresponds to the subgiant phase, where initially the envelope is completely radiative for this initial mass. The convective envelope starts to develop when the radius is already larger than  $10 R_{\odot}$ , leading to an almost fully convective envelope close to the tip of RGB. The horizontal gray dotted line corresponds to 0.33 in the right vertical axis (fraction of envelope mass that is convective). The core mass at the base of the RGB is taken from the radius at which this line intersects the blue points (gray vertical dotted line).

With this, it was possible to update Figure 3.7 by establishing the base of the RGB as a more likely minimum mass for sdBs descending from progenitors more massive than  $\sim 2.8 M_{\odot}$ . This result is shown in Figure 3.9 where the region colored in cyan shows the allowed masses for sdBs from MESA, while the red segmented region in-

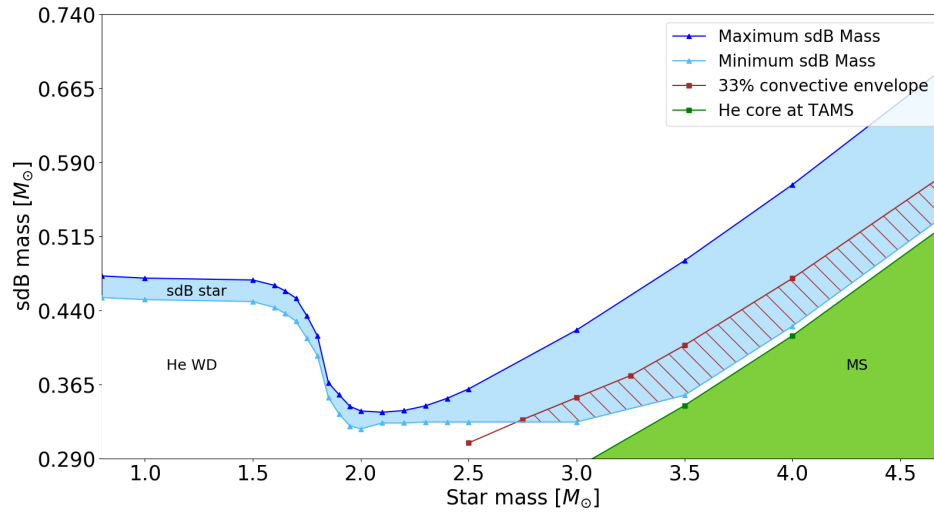


**Figure 3.9:** Same as Figure 3.7 but with the cyan region demarcating the range of sdBs. The red solid line represents the base of the RGB. The red hashed region corresponds to sdBs that could form from massive stars if they lose their envelopes during the subgiant branch, which is less likely than during the RGB phase. The green region corresponds to the MS.

indicates progenitors on the subgiant branch, which are less likely than progenitors on the RGB. I also show, as a reference, the green area that corresponds to core masses of stars that are still on the MS. The separation between the green and cyan regions corresponds to the  $0.01 M_{\odot}$  of hydrogen that I left around the core during the ‘Relax Mass’ process. Finally, stars that lose their envelope after the MS but before the core reaches the minimum mass needed to ignite helium and become sdB stars will become helium white dwarfs.

### 3.5.2 SdB masses for lower metallicity ( $Z = 0.004$ )

In order to compare with the results obtained by Han et al. (2002) for a lower metallicity, I have done the calculations with MESA for a grid with a metallicity of  $Z=0.004$  using the same parameters as in the grid of metallicity of  $Z=0.02$ , and only for the case with overshooting.

The comparison of the maximum sdB masses as a function of initial mass for the two metallicities from MESA is presented in Figure 3.10. The behavior is the same as obtained by Han et al. (2002, see Figure 2.2). For lower metallicity, the sdB masses are

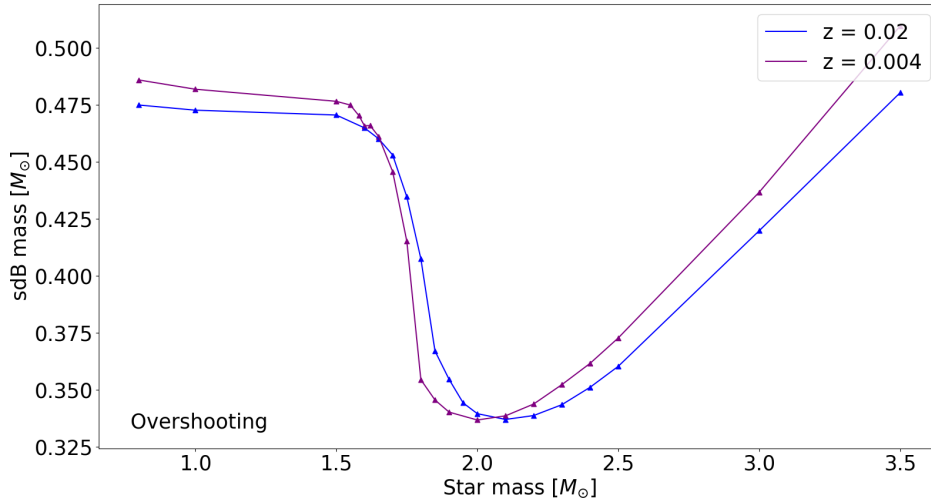


**Figure 3.10:** Comparison between the models with a solar metallicity (blue line) and with a metallicity  $z = 0.004$  (purple line) for the maximum sdB masses using the MESA code.

larger, except for the stars with initial masses in the range of  $\sim 1.6 - 2.0 M_{\odot}$ . A larger mass is expected for a lower metallicity because there is more hydrogen available to burn into helium during the MS, increasing the resulting helium-core mass. The initial mass range for which the maximum sdB mass is smaller than compared to the solar metallicity case, is caused by the reduction of the maximum initial mass for which the core becomes degenerate. This is an effect similar to that produced by the inclusion of overshooting (Figure 3.5) except that in this case the change in metallicity also affects masses lower than  $\sim 1.5 M_{\odot}$ .

Figure 3.11 shows the mass range of sdBs as a function of the initial mass for a metallicity of  $z = 0.004$  with overshooting. The behavior has the same tendency as in the two other models. For low initial masses (in range  $\sim 0.8 - 1.5 M_{\odot}$ ) the maximum mass of the sdBs is close to the canonical value ( $\sim 0.48 M_{\odot}$ ), then it begins to drop abruptly reaching a minimum for progenitor masses of  $\sim 1.9 - 2.1 M_{\odot}$ . For larger initial masses the maximum sdB mass begins to increase. In the same way for the values of the minimum sdB masses, the behavior is similar to that of the maximum sdB masses but typically  $\sim 0.02 M_{\odot}$  smaller up to initial masses of  $\sim 1.7 M_{\odot}$ . For initial masses larger than  $\sim 2.1 M_{\odot}$  the minimum sdB mass remains nearly constant, as in the case of solar metallicity, up to  $\sim 3 M_{\odot}$ . The minimum sdB mass for this model is  $0.308 M_{\odot}$ , which is smaller than the minimum sdB mass derived for massive

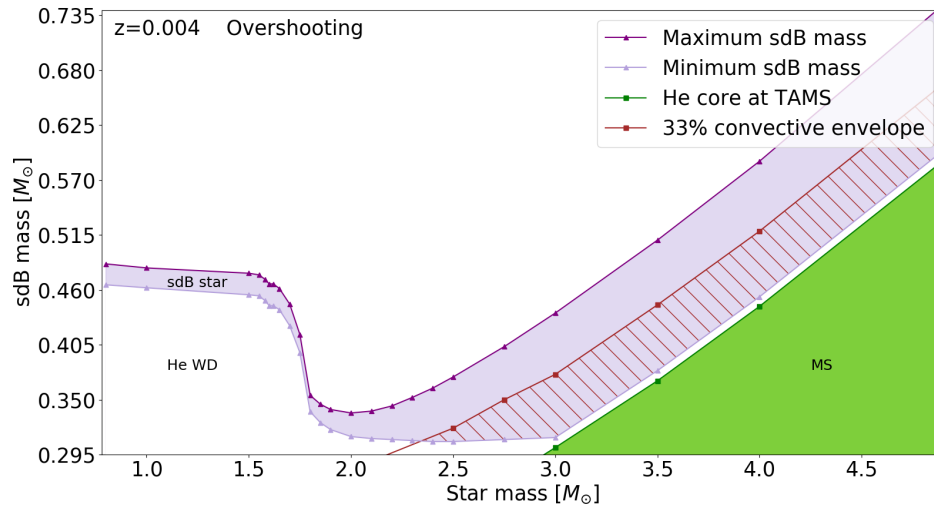


**Figure 3.11:** Same as in Figure 3.9 but for the MESA models with  $Z = 0.004$ . Purple and light purple triangles represent the results for the maximum and minimum sdB masses, respectively.

progenitors in the model with solar metallicity ( $0.327 M_{\odot}$ ). This is probably related to a higher concentration of helium in the core for the lower metallicity model, which allows lower-mass cores to ignite helium. For progenitors more massive than  $\sim 3 M_{\text{sun}}$ , the helium-core mass at the TAMS was already enough to ignite helium, and I again used this core mass plus the hydrogen envelope of  $0.01 M_{\text{sun}}$  as the minimum sdB mass.

The tables with the results obtained from MESA for the three models are presented in the appendix B.



# CHAPTER 4

## Discussion

The main objective of this chapter is to compare the results obtained here with the MESA code for the minimum and maximum sdB masses with those presented two decades ago by Han et al. (2002). I also analyze the duration of the sdB phase depending on the sdB mass and progenitor mass, and discuss the possible effects that this might have in binary populations synthesis models.

### 4.1 Comparison with the results from Han et al. (2002)

It is necessary to remember that the masses for the case without overshooting obtained by Han et al. (2002) do not include winds during the RGB phase, while all my models calculated with MESA include winds with a Reimer's mass loss factor of  $\eta = 0.25$ . However, as I mentioned in Section 2, the effect of the wind is not significant for the calculation of the sdB masses.

In Figure 4.1 I show the comparison of my results (in green) with those from Han et al. (2002, black and gray squares) for the case with  $Z = 0.02$  and without overshooting. The values obtained with MESA agree very precisely with those obtained by Han et al. (2002) with the Eggleton code, both for the maximum and minimum sdB masses. The only exception is for the more massive progenitor calculated by Han et al. (2002)

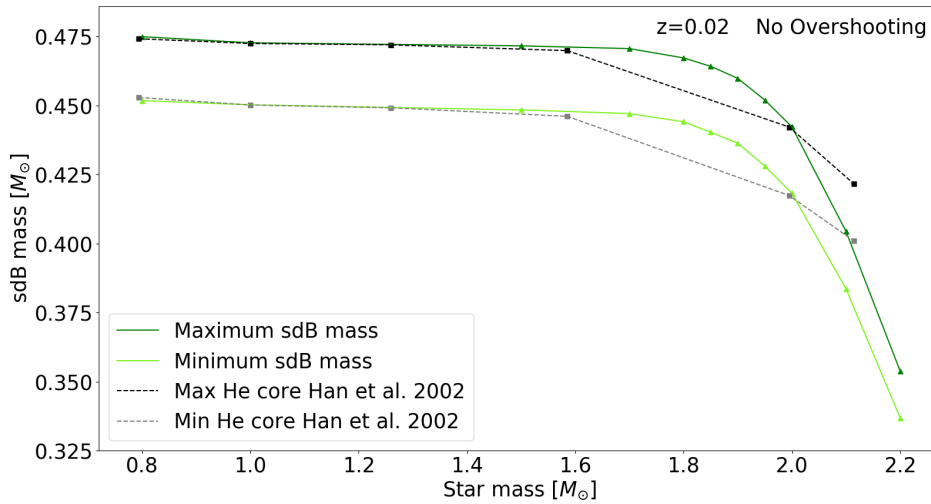


**Figure 4.1:** Same as in Figure 3.6 but including the values for the maximum (black) and minimum (gray) helium core that results in an sdB star from Han et al. (2002) for the models without overshooting and with a metallicity of  $z=0.02$ .

for this model, i.e. the one with  $\sim 2.1 M_{\odot}$ , for which I obtained smaller masses. Given that Han et al. (2002) did not simulate more massive progenitors in the models without overshooting, I can only conclude that the MESA and Eggleton’s codes are comparably good at doing stellar evolution for stars up to  $2.0 M_{\odot}$ . However, by having a much finer grid of progenitors in the MESA models, it was possible to smooth the drop in the curve that is obtained at the transition from stars that develop a degenerate core during the RGB to those that do not. For example, while the MESA models match the maximum and minimum sdB masses from Han et al. (2002) for  $\sim 1.6$  and  $\sim 2.0 M_{\odot}$ , the MESA calculations lie above the straight dashed lines that connect the values from Han et al. (2002) within this range. This implies that using a linear interpolation between those two initial masses from Han et al. (2002) would have resulted in an underestimation of the sdB masses within this range of progenitor masses.

The comparison for the case with overshooting and solar metallicity is presented in Figure 4.2, where the comparison can also be made for more massive progenitors. In this case, one can see that the values obtained with MESA agree very well with those of Han et al. (2002) for small initial masses ( $\lesssim 1.3 M_{\odot}$ ) that have a radiative core and for which convective core overshooting is not making any difference. For more massive stars, although the shape of the curves is similar, the values no longer fit as well. This

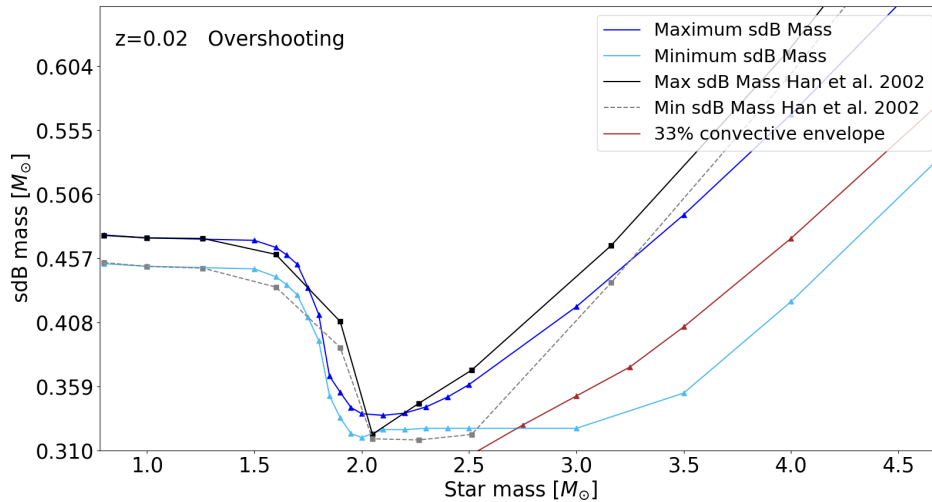


**Figure 4.2:** Same as in Figure 3.7 but including the values for the maximum (black) and minimum (gray) helium core that results in an sdB star from Han et al. (2002) for the models with overshooting and with a metallicity of  $Z = 0.02$ . I also included the red line that indicates the core mass at the base of the RGB calculated from MESA (assuming that 1/3 of the envelope is convective at this stage).

was expected since the prescriptions for overshooting used in both works are different. If we compare the prescription used by the Eggleton code (Eq. 2.1) with the one used in MESA (Eq. 3.2), the parameters that define overshooting are different and it is not easy to determine the relation between  $\delta_{ov}$  and  $f_{ov}$ . Looking at the range of initial masses for which the minimum and maximum masses for sdBs decrease abruptly, which occurs at slightly lower initial masses in my models, it appears that the MESA models with  $f_{ov} = 0.016$  have more overshooting than the models from Han et al. (2002) with  $\delta_{ov} = 0.12$ . Also, for initial masses between  $\sim 2.0$  and  $2.5M_{\odot}$ , the minimum sdB mass is nearly constant in both models, with the MESA models predicting a slightly larger minimum mass. This can also be related to a slightly stronger overshooting in the MESA models that allow for more massive cores. On the other hand, the maximum sdB mass seems to increase more abruptly after reaching the minimum in the results from Han et al. (2002), i.e. for stars that do not develop a degenerate core during the RGB phase, but this can be caused by the small number of models from Han et al. (2002) above  $2M_{\odot}$ . Finally, the minimum sdB masses from Han et al. (2002) for progenitors more massive than  $\sim 2.5M_{\odot}$  differ dramatically from the ones I derived.

For  $\sim 2.5 - 3.0 M_{\odot}$  I still obtain a constant minimum mass, while the minimum sdB masses derived by Han et al. (2002) start to increase in this range of progenitor masses. For more massive progenitors, the minimum sdB masses from my MESA models also start to increase again, but the values from Han et al. (2002) are much larger, resulting in a very narrow mass range for sdBs with a given progenitor mass. Even if I compare with the sdB masses at the base of the RGB that I calculated with MESA, assuming that it corresponds to the stage in the evolution where 1/3 of the envelope is convective, the derived sdB masses from Han et al. (2002) are much larger. This is in contrast to what I obtained in Section 2.1, where the core masses at the base of the RGB are calculated with the SSE code (which uses fits to stellar models from the Eggleton's code and has the same definition for the base of the RGB) were very close to the predicted minimum masses for sdBs from Han et al. (2002). Therefore, it can be concluded that MESA and the Eggleton's code do not agree above  $\sim 2.5 M_{\odot}$ , which may be related to the treatment of convection and/or overshooting. Considering that the MESA code is more updated and contains more physical parameters, and also that Han et al. (2002) presented only a few models for more massive stars, one might favour the results from MESA. In that case, the ranges of sdB masses for progenitors more massive than  $\sim 2 M_{\odot}$  are much wider than those calculated by Han et al. (2002).

The same exercise can be done for the case with a lower metallicity ( $Z = 0.004$ ) and with overshooting. Figure 4.3 compares the results obtained with MESA with the values obtained by Han et al. (2002). As in the case with solar metallicity, the maximum and minimum sdB masses are strongly consistent for low initial masses below  $\sim 1.3 M_{\odot}$  when the core is radiative and core overshooting has no effect. The drop of the curves from MESA in this model, matches the results from Han et al. (2002) much better than for the solar metallicity model. This could imply that the difference within the prescriptions for overshooting used in the Eggleton code and in MESA is smaller when lower metallicities are used. However, again for more massive progenitors than  $\sim 2 M_{\odot}$  the MESA models predict a different and wider range of masses for sdBs.

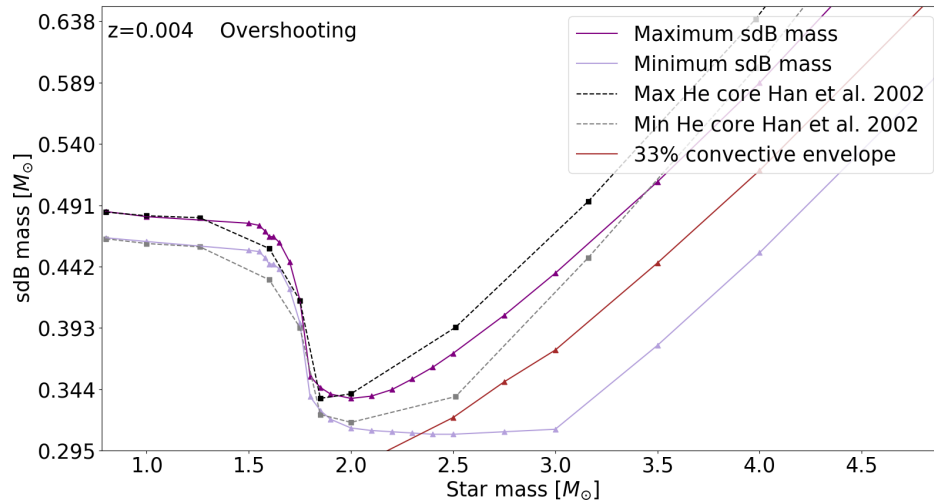


Figure 4.3: Same as in Figure 4.2 but for  $z=0.004$ .

## 4.2 Lifetimes of the sdBs

The duration of the sdB phase is an important aspect to consider when comparing simulations with observations. In Figures 4.4 and 4.5, I show the duration of the sdB phase obtained from the MESA models as a function of initial mass (left panel) and sdB mass (right panel), for the models with  $Z = 0.02$  and  $Z = 0.004$ , respectively. The most evident conclusion one can draw from these figures is that, regardless of the metallicity, the duration of the sdB phase is strongly dependent on the sdB mass, decreasing for more massive sdBs. More massive sdBs are hotter, and therefore burn faster, which results in a shorter lifetime. The calculated lifetimes fit extremely well with a linear fit in the  $\log(\text{Time}) - \log(M_{\text{sdb}})$  plane. The fit is represented by the solid lines in the right panels of both figures (the figures are not in a logarithmic scale). This behaviour is consistent with the sdB lifetime as a function of sdB mass given by Yungelson (2008). The main difference within the two models is that in the low metallicity case the the least massive sdBs are  $0.02 M_{\odot}$  less massive than in the models with  $Z = 0.02$ , so that the longest lifetimes exceed 1 Gyr for  $Z = 0.004$ .

With respect to the duration of the sdB phase as a function of the initial mass, however, the analysis depends on whether we look at the behaviour for the minimum or maximum sdB masses.

For the minimum sdB masses the duration of the sdB phase does not show an over-

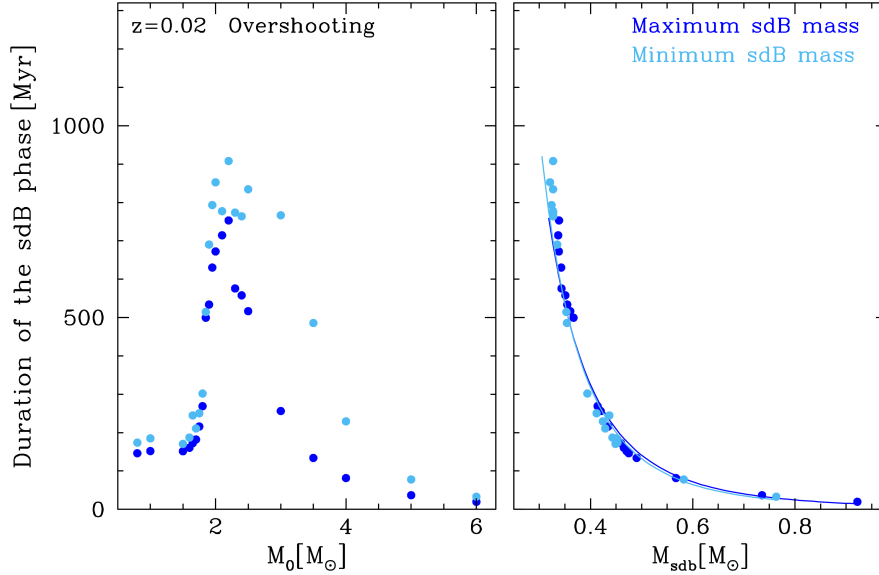


**Figure 4.4:** Duration of the sdB phase as a function of the initial mass (*left*) and sdB mass (*right*) for the models with  $Z = 0.02$  and overshooting. The blue dots correspond to the maximum sdB masses (i.e. removing the envelope at the tip of the RGB), while the light blue dots are for the minimum sdB masses. The solid lines in the right panel correspond to a linear fit to the data in a log – log scale.

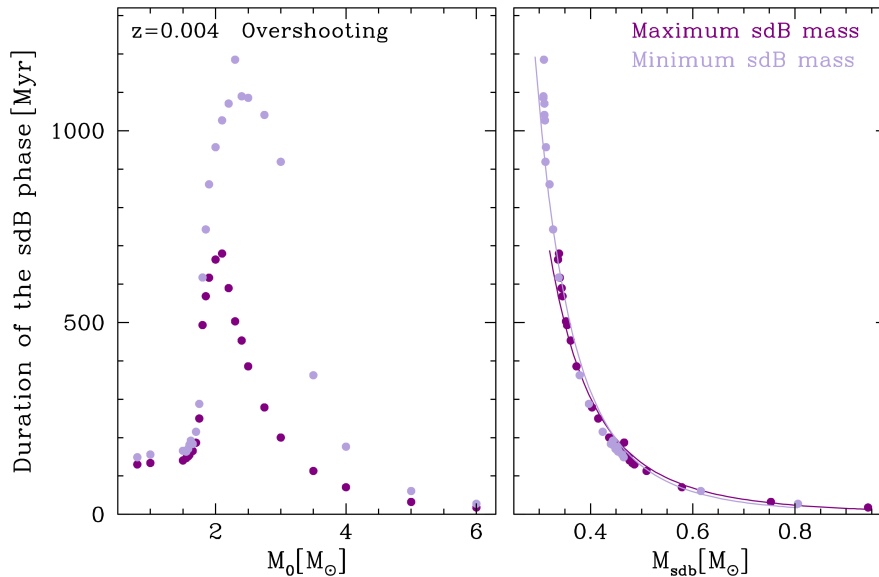


**Figure 4.5:** Same as in Figure 4.4 but for  $Z = 0.004$ .

all tendency as a function of initial mass but a sharp change from a typical duration of  $\sim 150 - 200$  Myr for stars with low initial masses ( $\lesssim 2 M_{\text{sun}}$ ), where the core of the star

becomes degenerate during the RGB phase, to  $\sim 800 - 900$  Myr (for  $Z = 0.02$ ) or even larger than 1000 Myr (for  $Z = 0.004$ ) for more massive progenitors that ignite helium smoothly. This is directly related to the drop in the minimum sdB mass near  $\sim 2 M_{\odot}$  seen in all the models discussed in this thesis.

For the maximum sdB masses, the duration of the sdB phase as a function of the initial mass behaves in a very similar way for stars with initial masses  $\lesssim 2 M_{\odot}$ , with the clear sharp increase in the sdB phase duration around initial masses where the core stops becoming degenerate during the RGB. However, for progenitors with  $M_0 \gtrsim 2.5 M_{\odot}$  the duration of the sdB phase decreases continuously with initial mass, as a consequence of the increase in the maximum sdB mass for more massive progenitors.

Considering the derived duration of the sdB phase which increases as decreasing the sdB mass, as well as the mass range for sdBs derived in the previous Chapter which is larger for more massive progenitors, the observed mass distribution for sdB stars (e.g. Figure 1.3) is a clear reflection of the initial mass function. If the initial mass function were flat, i.e. all initial masses were equally likely, one would expect the mass distribution of sdBs to peak at lower masses ( $\sim 0.3 - 0.4 M_{\odot}$ ). However, it is widely accepted from the initial mass function (e.g., Kroupa, 2001) that low-mass stars are much more likely to form. Therefore, most sdBs should descend from progenitors with initial masses  $\lesssim 1.5 M_{\odot}$ , resulting in an sdB mass distribution that peaks at the canonical value, with a tail towards lower sdB masses (descending from progenitors with initial masses of  $\sim 2 - 3 M_{\odot}$ ) and a smaller tail towards more massive sdBs (that descend from the more massive, and less common, stars). This is the behaviour one can see in Figure 1.3, although it should be taken with caution due to the low number of statistics (only 22 systems).

### 4.3 Implications for binary modelling

Binary population synthesis models should consider all the factors that might affect the sdB mass distribution in order to compare with observations. In what follows I discuss some of these.

- 1) The range of possible core masses that result in an sdB star after losing the envelope, translates into a range of radii where a star can fill its Roche lobe to become an sdB, constraining the range of initial orbital periods.

2) The lifetime of an sdB strongly depends on its mass, as I discuss in Section 4.2, with low-mass sdBs spending more time in this phase.

3) The age of the population is also a crucial factor to consider in simulations that attempt to compare with observational samples of sdBs. Low-mass stars need much longer to leave the main sequence and become giants, i.e. possible sdB progenitors, compared to more massive stars. Also, old (low-metallicity) stars evolve faster than their younger (high-metallicity) counterparts. Therefore, a very old and low metallicity population, for example from the halo of the Milky Way, will probably have an sdB mass distribution strongly peaked at the canonical mass. This peak should become less pronounced as we move into younger populations.

4) The metallicity also has a small but not negligible effect on the sdB masses. However, the metallicity strongly affects the minimum initial mass that can evolve from the MS at a given age. For example, a star of  $0.8 M_{\odot}$  with solar metallicity does not have enough time to leave the MS within the Hubble time, but if the same star has a very low metallicity (e.g.,  $Z = 0.0005$ ) it will evolve faster and will be able to leave the MS within the Hubble time (based on simulations with the SSE code, Hurley et al. 2000).

5) The inclusion of core overshooting during the MS, increases the resulting sdB mass for progenitors more massive than  $\sim 1.5 M_{\odot}$ . However, different prescriptions for overshooting are available, without a general consensus on the more suitable. Also, the extent of the overshoot region ( $f_{ov}$ ) is another parameter that remains poorly constrained. Although  $f_{ov} = 0.016$  seems to fit well for stars more massive than  $2 M_{\odot}$ , Claret & Torres (2016, 2017, 2018, 2019) suggest that there is a dependence of the strength of overshooting on stellar mass, with a sharp increase between  $\sim 1.2$  and  $\sim 2 M_{\odot}$ . This conclusion, however, is still under debate (e.g., Constantino & Baraffe, 2018).

6) The likelihood of a star to have a binary companion, which is a necessary ingredient to form sdB stars, should also be considered. There is observational evidence that the overall binary frequency is an increasing function of stellar mass (e.g., Raghavan et al., 2010).

7) It should also be taken into account whether the observed population consists of single sdBs or sdBs in wide or close binary systems. Close sdB binaries are most certainly the result of common envelope evolution, in which the envelope is rapidly ejected during the RGB phase. On the other hand, sdBs in binaries with periods of hundreds of days probably descend from a previous phase of stable mass transfer.

A considerably larger timescale is needed in order to eject the envelope in the later scenario. The different timescales involved might have a measurable effect on the resulting sdB star, for example on the mass of the hydrogen envelope that is retained. For the population of single sdBs, which are expected to descend from a merger process, the internal structure of the sdBs is probably affected, and the mass distribution for this population might be completely different.

8) SdBs in binary systems can be paired with different types of companions, that might also influence the sdB masses. For example, Schaffenroth et al. (2022) suggests that the observed sdBs in close binaries show a different sdB mass distribution if they are paired with un-evolved low-mass companions, i.e. M dwarfs or brown dwarfs, or with white dwarf companions. While the sdBs with M dwarf or brown dwarf companions show a peak around the canonical mass, the peak of the distribution is shifted to lower masses for sdBs with white dwarf companions. The latter probably underwent two mass transfer phases, with the first phase caused by the evolution of the white dwarf progenitor, which must have affected the orbital period of the system before the second mass transfer phase and/or the mass of the sdB progenitor.

Having taken all these aspects of stellar population into account one might obtain a realistic mass distribution of the present Galactic sdB population.



# CHAPTER 5

## Summary and Future Work

The purpose of this chapter is to highlight the main points of this thesis and the results derived from it. In addition, I propose possible future work to improve the current knowledge and new objectives to further deepen the area of research on hot sdB stars.

According to the mass range obtained in this work (see Tables B.2 and Tables B.3) low-mass stars ( $\lesssim 1.5 M_{\odot}$ ) result in sdB stars with masses in the range of  $\sim 0.450 - 0.475 M_{\odot}$  for solar metallicities and  $\sim 0.455 - 0.486 M_{\odot}$  for  $Z = 0.004$ , i.e. clustering around the canonical sdB mass. SdBs with smaller masses descend from progenitors with initial masses of  $\sim 2.0 - 3.0 M_{\odot}$ , while high-mass sdBs come from initial mass  $\gtrsim 3.5 M_{\odot}$ .

The inclusion of overshooting is very important for sdBs descending from progenitors more massive than  $\sim 1.5 M_{\odot}$ . Models with overshooting predict more massive helium cores at the end of the main sequence, which determines the evolution during the RGB phase, the mass of the helium core at the tip, and the maximum progenitor mass for which helium is ignited under degenerate conditions. Including overshooting decreases the maximum progenitor mass for which the core becomes degenerate during the RGB phase. This causes the sdBs to have a smaller mass for progenitors in the range of  $\sim 1.5 - 2.3 M_{\odot}$  and a larger mass for more massive progenitors, compared with the models without overshooting, in agreement with the results previously presented by Ostrowski et al. (2021).

Changing the metallicity also affects the range of possible sdB masses and the max-

imum mass for progenitors that develop a degenerate core during the RGB phase, but the effect is less pronounced than that of overshooting. The models with  $Z = 0.004$  predict, in general, slightly larger sdB masses (typically  $\sim 0.01 - 0.02 M_{\odot}$  larger) than the models with  $Z = 0.02$ .

I also found that the duration of the sdB phase is strongly dependant on the sdB mass, with the less massive sdBs ( $M_{\text{sdB}} \sim 0.3 M_{\odot}$ ) spending  $\sim 2$  orders of magnitudes more time on the sdB phase than the more massive sdBs ( $M_{\text{sdB}} > 0.9 M_{\odot}$ ). One might think, therefore, that low-mass sdBs should be more common among the observed systems. However, the observed sdB mass distribution (e.g. Fontaine et al., 2012) peaks at the canonical mass, which means that the initial mass function has a much stronger effect than the sdB lifetime on the sdB mass distribution.

Several factors need to be considered in binary population synthesis models in order to reproduce the observed sdB mass distribution like: metallicity, core overshooting, the initial mass function for the progenitor of the sdBs, the mass ratio, the range of initial orbital periods, the age of the population, the sdB lifetime depending on its mass, the likelihood of a star to have a binary companion, and any other property that might affect the sdB masses.

The results derived in this thesis are important to deepen the study of sdB stars because these can be used, for example, in binary population synthesis models or to constrain the evolution of observed sdBs with accurate mass measurements.

I have shown that the metallicity assumed for the progenitors has a small but not negligible effect on the final sdB mass. Therefore, in the future, I intend to repeat all the calculations with different metallicities in order to generate grids that can be used in simulations.

Also, I confirmed the results previously presented by Ostrowski et al. (2021) on the effects of the inclusion of overshooting in the models. The mass of the helium core of the progenitor star is strongly affected by the inclusion of core overshooting during the MS, therefore affecting the final sdB mass. I want to investigate further into the use of overshooting and explore models with the different overshooting prescriptions available in MESA and the effect of changing some of the input parameters, like  $f_0$ .

Having already fine grids for sdB masses as a function of the initial mass for different metallicities and overshooting strengths/prescriptions, it will be possible to use binary population synthesis models to simulate the population of the different types of sdBs: close (post common envelope) sdB binaries, wide (post stable mass transfer)

---

sdB binaries, and single (post-merger) sdBs. At least for sdBs in binary systems, I already have a path in mind to follow:

- Post common envelope binaries can be simulated using the binary star evolution code (BSE) from Hurley et al. (2002), as it has been done by, e.g., Camacho et al. (2014); Zorotovic et al. (2014) for close white dwarfs + main sequence binaries. An application to sdBs in close binaries was included in Zorotovic & Schreiber (2013), applying filters to the binary population simulated with BSE, based on the mass ranges from Han et al. (2002). Given that I was recently accepted to do a Ph.D. at the University of Valparaíso, under the supervision of Dr. Zorotovic, I expect to learn how to use BSE to perform my own simulations, including the constraints on the mass ranges derived from this work.
- For wide binaries I want to use MESA to perform a statistically significant binary population synthesis study, as it has been done in Vos et al. (2020). This work will be performed in close collaboration with my co-supervisor Dr. Maja Vučković, and her collaborators Dr. Alexey Bobrick (external reviewer of this thesis) and Dr. Joris Vos.

The main objective from these simulations will be to reproduce the mass distribution of sdB stars and compare with the current observational results, for different populations (wide/close binaries), considering also the metallicity and age of the different environments.

I would also like to redo some of the models using a slower mass-loss rate instead of the 'Relax Mass' process. In this work I have found that the process used is equivalent to applying a high mass-loss rate,  $10^{-3} - 10^{-2} M_{\odot}/\text{year}$ , which results in a loss of the envelope on a time scale of the order of 1000 years. By applying a lower mass loss rate, e.g.  $10^{-6} - 10^{-5} M_{\odot}/\text{year}$ , I could compare if there is any difference in sdBs that belong to close (post common envelope) or wide (post stable mass transfer) binaries.

Another straightforward project will be to reconstruct the previous evolution of eclipsing sdB + non-evolved (MS or brown dwarf) companions in order to constrain the efficiency of the common envelope phase, as it has been done in, e.g., Zorotovic et al. (2010); Zorotovic & Schreiber (2022), but using the constraints on the initial mass range from the sdB masses.



# APPENDIX A

## MESA inlists

Here I give one example for each of the three inlist files. The star in all these samples has the same initial mass ( $1 M_{\odot}$ ) and metallicity ( $Z = 0.004$ ) and the envelope was extracted when the core mass was  $M_c = 0.452 M_{\odot}$ .

### A.1 Pre-MS to TAMS

```
! inlist to evolve a  $1 M_{\odot}$  star from the pre-MS to the TAMS.

&star_job
! see star/defaults/star_job.defaults
! begin with a pre-main sequence model
create_pre_main_sequence_model = .true.

! save a model at the end of the run
save_model_when_terminate = .true.
save_model_filename = 'sdB1.0M_at_TAMS.mod'

! display on-screen plots
pgstar_flag = .true.

/ ! end of star_job namelist

&eos
```

```

! eos options
! see eos/defaults/eos.defaults

/ ! end of eos namelist

&kap
! kap options
! see kap/defaults/kap.defaults
use_Type2_opacities = .true.
Zbase = 0.004

/ ! end of kap namelist

&controls
! see star/defaults/controls.defaults
! starting specifications
initial_mass = 1.0 ! in Msun units
initial_z = 0.004

! options for energy conservation
use_dedt_form_of_energy_eqn = .true.
use_gold_tolerances = .true.

!max_years_for_timestep = 5d6
!mesh_delta_coeff = 0.5

! The non-default mixing parameters:
mixing_length_alpha = 1.8d0 ! The Henyey theory of convection
MLT_option = 'Cox'
use_Ledoux_criterion = .true.

! The 'predictive mixing' scheme
predictive_mix(1) = .true.
predictive_zone_type(1) = 'any'
predictive_zone_loc(1) = 'core'
predictive_bdy_loc(1) = 'any'
predictive_superad_thresh(1) = 0.005
predictive_mix(2) = .true.
predictive_zone_type(2) = 'any'
predictive_zone_loc(2) = 'surf'

```

```

predictive_bdy_loc(2) = 'any'
predictive_superad_thresh(2) = 0.001

! Core overshoot
overshoot_scheme(1) = 'exponential'
overshoot_zone_type(1) = 'any'
overshoot_zone_loc(1) = 'core'
overshoot_bdy_loc(1) = 'top'
overshoot_f(1) = 0.016
overshoot_f0(1) = 0.008
overshoot_mass_full_off(1) = 1.10
overshoot_mass_full_on(1) = 1.30

!Stop at the TAMS
xa_central_lower_limit_species(1) = 'h1'
xa_central_lower_limit(1) = 1d-4

/ ! end of controls namelist

```

## A.2 TAMS to the tip of the RGB

```

! inlist to evolve a  $1M_{\odot}$  star from the TAMS to the tip of the RGB.

&star_job
! see star/defaults/star_job.defaults
! Load a previous model to run
load_saved_model = .true.
saved_model_name = 'sdB1.0M_at_TAMS.mod'
! save a model at the end of the run
save_model_when_terminate = .true.
! File name for stopping at a given core mass.
save_model_filename = 'sdB1.0M_at_RGB_0.452Hecore.mod'
! Alternatively, file name for stopping at at the tip of the RGB.
! save_model_filename = 'sdB1.0M_at_TRGB.mod'
! display on-screen plots
pgstar_flag = .true.

/ ! end of star_job namelist

```

```

&eos
  ! eos options
  ! see eos/defaults/eos.defaults
/ ! end of eos namelist

&kap
  ! kap options
  ! see kap/defaults/kap.defaults
  use_Type2_opacities = .true.
  Zbase = 0.004d0
/ ! end of kap namelist

&controls
  ! see star/defaults/controls.defaults
  ! starting specifications
  initial_mass = 1.0 ! in Msun units
  initial_z = 0.004d0

  ! options for energy conservation
  use_dedt_form_of_energy_eqn = .true.
  use_gold_tolerances = .true.
  !max_years_for_timestep = 5d6
  !mesh_delta_coeff = 0.5
  photo_interval= 100

  ! The non-default mixing parameters:
  mixing_length_alpha = 1.8d0 ! The Henyey theory of convection
  MLT_option = 'Cox'
  use_Ledoux_criterion = .true.

  ! The 'predictive mixing' scheme
  predictive_mix(1) = .true.
  predictive_zone_type(1) = 'any'
  predictive_zone_loc(1) = 'core'
  predictive_bdy_loc(1) = 'any'
  predictive_superad_thresh(1) = 0.005
  predictive_mix(2) = .true.
  predictive_zone_type(2) = 'any'

```

```
predictive_zone_loc(2) = 'surf'
predictive_bdy_loc(2) = 'any'
predictive_superad_thresh(2) = 0.001

! Wind in te RGB path evolution
!cool_wind_full_on_T = 9.99d9
!hot_wind_full_on_T = 1d10
cool_wind_RGB_scheme = 'Reimers'
!cool_wind_AGB_scheme = 'Blocker'
!RGB_to_AGB_wind_switch = 1d-4
Reimers_scaling_factor = 0.25d0
!Blocker_scaling_factor = 0.0003d0

! Stop at a specific model number (that corresponds to a fixed helium
core mass)
max_model_number = 9850 ! Model number for  $M_c = 0.452 M_{\odot}$ .
! Alternatively, Stop at the tip of the RGB
!power_he_burn_upper_limit = 10d0

/ ! end of controls namelist
```

## A.3 Removing the envelope and evolving until the white dwarf cooling track

```
! inlist to remove the envelope for a  $1M_{\odot}$  star on the RGB, at a given
helium core mass (in this sample  $0.452M_{\odot}$ ), to the WD cooling track

&star_job
! see star/defaults/star_job.defaults
! Load a previous model to run
load_saved_model = .true.
saved_model_name = 'sdB1.0M_at_RGB_0.452Hecore.mod'
! save a model at the end of the run
save_model_when_terminate = .true.
save_model_filename = 'sdB1.0M_0.452Hecore_at_WD.mod'
! display on-screen plots
```

```

pgstar_flag = .true.
! Relax the mass to the sdB mass
relax_mass = .true.
relax_initial_mass= .false.
new_mass = 0.462
lg_max_abs_mdot = -100
/ ! end of star_job namelist

&eos
! eos options
! see eos/defaults/eos.defaults
/ ! end of eos namelist

&kap
! kap options
! see kap/defaults/kap.defaults
use_Type2_opacities = .true.
Zbase = 0.004d0
/ ! end of kap namelist

&controls
! see star/defaults/controls.defaults
! starting specifications
initial_mass = 1.0 ! in Msun units
initial_z = 0.004d0

! options for energy conservation
use_dedt_form_of_energy_eqn = .true.
use_gold_tolerances = .true.

photo_interval= 250
photo_digits = 5
history_interval = 1

! Relax convergence criteria (needed during flash)
convergence_ignore_eqnL_residuals = .true.
min_timestep_limit = 1d-30
varcontrol_target = 1d-4

```

### A.3. REMOVING THE ENVELOPE AND EVOLVING UNTIL THE WHITE DWARF COOLING TRACK

---

```
! The non-default mixing parameters:
mixing_length_alpha = 1.8d0 ! The Henyey theory of convection
MLT_option = 'Cox'
use_Ledoux_criterion = .true.

! The 'predictive mixing' scheme
predictive_mix(1) = .true.
predictive_zone_type(1) = 'any'
predictive_zone_loc(1) = 'core'
predictive_bdy_loc(1) = 'any'
predictive_superad_thresh(1) = 0.005

predictive_mix(2) = .true.
predictive_zone_type(2) = 'any'
predictive_zone_loc(2) = 'surf'
predictive_bdy_loc(2) = 'any'
predictive_superad_thresh(2) = 0.001

! Stopping criteria
log_L_lower_limit = -3.5
/ ! end of controls namelist
```



# APPENDIX B

## Tables

The values obtained with MESA are presented in the next tables. For each initial mass ( $M_0$ ) I listed the minimum and maximum sdB masses ( $M_{\text{sdB}}^{\min}$  and  $M_{\text{sdB}}^{\max}$ , respectively) and the corresponding duration of the sdB phase for both limits ( $t_{\text{sdB}}^{\min}$  and  $t_{\text{sdB}}^{\max}$ ).

## B.1 SdB properties for solar metallicity without overshooting

**Table B.1:** Models with  $Z = 0.02$  and without overshooting. For progenitors more massive than  $2.2 M_{\odot}$  I did not calculate the minimum SdBs masses (see Section 3.5.1).

$M_0 [M_{\odot}]$	$M_{\text{sdB}}^{\text{min}} [M_{\odot}]$	$M_{\text{sdB}}^{\text{max}} [M_{\odot}]$	$t_{\text{sdB}}^{\text{min}} [\text{Myr}]$	$t_{\text{sdB}}^{\text{max}} [\text{Myr}]$
0.80	0.453	0.4748	173.771	154.022
1.00	0.451	0.4727	184.897	149.934
1.50	0.449	0.4716	178.629	152.506
1.70	0.448	0.4706	181.738	149.448
1.80	0.445	0.4673	179.570	161.846
1.85	0.441	0.4642	199.439	162.302
1.90	0.437	0.4598	196.891	169.299
1.95	0.429	0.4520	213.385	180.573
2.00	0.419	0.4422	114.565	248.287
2.10	0.386	0.4043	343.094	295.000
2.20	0.339	0.3537	648.363	518.556
2.30	-	0.3374	-	732.814
2.40	-	0.3328	-	714.750
2.50	-	0.3341	-	855.215
2.60	-	0.3389	-	633.042
2.70	-	0.3459	-	583.882
2.80	-	0.3544	-	510.543
2.90	-	0.3642	-	454.152
3.00	-	0.3743	-	387.191
3.10	-	0.3849	-	349.432
3.20	-	0.3955	-	316.420
3.30	-	0.4071	-	275.064
3.40	-	0.4188	-	280.229
3.50	-	0.4309	-	222.873

## B.2 SdB properties for solar metallicity with overshooting

**Table B.2:** Model with  $Z = 0.02$  and with overshooting. The last four values for the minimum sdB masses (highlighted with \*) correspond to the helium core mass at the end of the MS plus the  $0.01M_{\odot}$  of hydrogen initially left in our models, as explained in Section 3.5.1.

$M_0 [M_{\odot}]$	$M_{\text{sdB}}^{\text{min}} [M_{\odot}]$	$M_{\text{sdB}}^{\text{max}} [M_{\odot}]$	$t_{\text{sdB}}^{\text{min}} [\text{Myr}]$	$t_{\text{sdB}}^{\text{max}} [\text{Myr}]$
0.80	0.453	0.4750	173.816	146.229
1.00	0.451	0.4727	184.991	151.853
1.50	0.449	0.4708	170.595	151.447
1.60	0.443	0.4654	187.118	160.581
1.65	0.437	0.4598	244.766	172.555
1.70	0.429	0.4525	210.791	182.086
1.75	0.412	0.4347	250.455	216.005
1.80	0.394	0.4141	301.926	268.925
1.85	0.352	0.3669	514.440	499.495
1.90	0.335	0.3546	690.188	533.812
1.95	0.323	0.3429	793.181	630.290
2.00	0.320	0.3382	852.508	672.291
2.10	0.326	0.3369	777.180	714.341
2.20	0.326	0.3386	907.959	753.083
2.30	0.327	0.3434	773.523	575.766
2.40	0.327	0.3509	763.895	557.824
2.50	0.327	0.3605	834.353	516.543
3.00	0.327	0.4201	766.546	256.288
3.50	0.354*	0.4904	485.733	133.992
4.00	0.424*	0.5673	229.329	81.607
5.00	0.583*	0.7356	77.889	36.857
6.00	0.764*	0.9221	32.992	19.696

### B.3 sdB properties for $Z = 0.004$ metallicity with overshooting

**Table B.3:** Model with  $Z = 0.004$  and with overshooting. As in Table B.2, the values with \* correspond to the helium core mass at the end of the MS plus the  $0.01M_{\odot}$  of hydrogen initially left in our models.

$M_0 [M_{\odot}]$	$M_{\text{sdb}}^{\text{min}} [M_{\odot}]$	$M_{\text{sdb}}^{\text{max}} [M_{\odot}]$	$t_{\text{sdb}}^{\text{min}} [\text{Myr}]$	$t_{\text{sdb}}^{\text{max}} [\text{Myr}]$
0.80	0.465	0.4860	148.898	130.162
1.00	0.462	0.4819	155.960	133.928
1.50	0.455	0.4766	165.632	140.454
1.55	0.454	0.4749	163.483	146.724
1.58	0.449	0.4703	170.491	150.974
1.60	0.444	0.4658	180.844	155.250
1.62	0.444	0.4659	192.068	187.179
1.65	0.440	0.4612	183.682	165.298
1.70	0.424	0.4457	215.270	186.715
1.75	0.397	0.4152	287.963	249.861
1.80	0.338	0.3543	617.412	493.391
1.85	0.327	0.3454	742.781	568.621
1.90	0.320	0.3401	860.261	616.861
2.00	0.313	0.3366	957.037	664.263
2.10	0.311	0.3385	1027.066	679.869
2.20	0.310	0.3437	1070.853	589.696
2.30	0.309	0.3522	1185.198	503.220
2.40	0.308	0.3615	1089.799	453.181
2.50	0.308	0.3727	1085.671	385.872
2.75	0.310	0.4031	1041.204	278.782
3.00	0.312*	0.4367	918.954	200.273
3.50	0.379*	0.5097	362.658	113.173
4.00	0.453*	0.5788	176.400	70.684
5.00	0.616*	0.7531	60.871	32.398
6.00	0.806*	0.9430	27.678	17.829

# Bibliography

- Camacho J., Torres S., García-Berro E., Zorotovic M., Schreiber M. R., Rebassa-Mansergas A., Nebot Gómez-Morán A., Gänsicke B. T., 2014, *A&A*, 566, A86
- Claret A., Torres G., 2016, *A&A*, 592, A15
- Claret A., Torres G., 2017, *ApJ*, 849, 18
- Claret A., Torres G., 2018, *ApJ*, 859, 100
- Claret A., Torres G., 2019, *ApJ*, 876, 134
- Constantino T., Baraffe I., 2018, *A&A*, 618, A177
- Eggleton P. P., 1971, *MNRAS*, 151, 351
- Eggleton P. P., 1972, *MNRAS*, 156, 361
- Eggleton P. P., 1973, *MNRAS*, 163, 279
- Fontaine G., Brassard P., Charpinet S., Green E. M., Randall S. K., Van Grootel V., 2012, *A&A*, 539, A12
- Ghasemi H., Moravveji E., Aerts C., Safari H., Vučković M., 2017, *MNRAS*, 465, 1518
- Greenstein J. L., 1956, in *Third Berkeley Symposium on Mathematical Statistics and Probability*, p. 11
- Han Z., Podsiadlowski P., Eggleton P. P., 1995, *MNRAS*, 272, 800
- Han Z., Podsiadlowski P., Maxted P. F. L., Marsh T. R., Ivanova N., 2002, *MNRAS*, 336, 449
- Heber U., 2009, *ARA&A*, 47, 211
- Heber U., 2016, *PASP*, 128, 082001

## BIBLIOGRAPHY

---

- Herwig F., 2000, *A&A*, 360, 952
- Humason M. L., Zwicky F., 1947, *ApJ*, 105, 85
- Hurley J. R., Pols O. R., Tout C. A., 2000, *MNRAS*, 315, 543
- Hurley J. R., Tout C. A., Pols O. R., 2002, *MNRAS*, 329, 897
- Iben J., I., Tutukov A. V., 1985, *ApJS*, 58, 661
- Iben J., Icko, Tutukov A. V., 1986, *ApJ*, 311, 753
- Jermyn A. S. et al., 2023, *ApJS*, 265, 15
- Justham S., Podsiadlowski P., Han Z., 2010, *Monthly Notices of the Royal Astronomical Society*, 410, 984
- Kroupa P., 2001, *MNRAS*, 322, 231
- Krtićka J., Kubát J., Krtićková I., 2016, *A&A*, 593, A101
- Kuiper G. P., 1939, *ApJ*, 89, 548
- Luyten W. J., 1953, *AJ*, 58, 75
- Morgan W. W., Keenan P. C., Kellman E., 1943, *An atlas of stellar spectra, with an outline of spectral classification*
- Münch G., 1958, *ApJ*, 127, 642
- Ostrowski J., Baran A. S., Sanjayan S., Sahoo S. K., 2021, *MNRAS*, 503, 4646
- Paczynski B., 1976, in *IAU Symposium, Vol. 73*, Eggleton P., Mitton S., Whelan J., eds, *Structure and Evolution of Close Binary Systems*, p. 75
- Paxton B., Bildsten L., Dotter A., Herwig F., Lesaffre P., Timmes F., 2011, *ApJS*, 192, 3
- Paxton B. et al., 2013, *ApJS*, 208, 4
- Paxton B. et al., 2015, *ApJS*, 220, 15
- Paxton B. et al., 2018, *ApJS*, 234, 34
- Paxton B. et al., 2019, *ApJS*, 243, 10
- Pedersen M. G., Aerts C., Pápics P. I., Rogers T. M., 2018, *A&A*, 614, A128

- Pelisoli I., Vos J., Geier S., Schaffenroth V., Baran A. S., 2020, *A&A*, 642, A180
- Perets H. B., Zenati Y., Toonen S., Bobrick A., 2019, arXiv e-prints, arXiv:1910.07532
- Pols O. R., Schröder K.-P., Hurley J. R., Tout C. A., Eggleton P. P., 1998, *MNRAS*, 298, 525
- Pols O. R., Tout C. A., Schroder K.-P., Eggleton P. P., Manners J., 1997, *MNRAS*, 289, 869
- Raghavan D. et al., 2010, *ApJS*, 190, 1
- Schaffenroth V., Pelisoli I., Barlow B. N., Geier S., Kupfer T., 2022, *A&A*, 666, A182
- Schaller G., Schaerer D., Meynet G., Maeder A., 1992, *A&AS*, 96, 269
- Scherbak P., Fuller J., 2023, *MNRAS*, 518, 3966
- Schindler J.-T., Green E. M., Arnett W. D., 2015, *ApJ*, 806, 178
- Schroder K.-P., Pols O. R., Eggleton P. P., 1997, *MNRAS*, 285, 696
- Taylor J. H., Fowler L. A., McCulloch P. M., 1979, *Nature*, 277, 437
- Vos J., Bobrick A., Vučković M., 2020, *A&A*, 641, A163
- Vos J., Vučković M., Chen X., Han Z., Boudreaux T., Barlow B. N., Østensen R., Németh P., 2019, *MNRAS*, 482, 4592
- Webbink R. F., 1984, *ApJ*, 277, 355
- Xiong H., Chen X., Podsiadlowski P., Li Y., Han Z., 2017, *A&A*, 599, A54
- Yungelson L. R., 2008, *Astronomy Letters*, 34, 620
- Zenati Y., Toonen S., Perets H. B., 2019, *MNRAS*, 482, 1135
- Zhang Q.-S., Christensen-Dalsgaard J., Li Y., 2022, *MNRAS*, 512, 4852
- Zorotovic M., Schreiber M., 2022, *MNRAS*, 513, 3587
- Zorotovic M., Schreiber M. R., 2013, *A&A*, 549, A95
- Zorotovic M., Schreiber M. R., Gänsicke B. T., Nebot Gómez-Morán A., 2010, *A&A*, 520, A86
- Zorotovic M., Schreiber M. R., García-Berro E., Camacho J., Torres S., Rebassa-Mansergas A., Gänsicke B. T., 2014, *A&A*, 568, A68